High-Altitude Aircraft and Balloon-Borne Observations of OH, HO_2, ClO, BrO, NO_2, $ClONO_2$, ClOOCl, H_2O, and O_3 in Earth's Stratosphere

Summary of Research
NASA Langley Agreement NAG-1-1305
July 1, 1991–December 31, 1998

Submitted to
National Aeronautics and Space Administration
from
President and Fellows of Harvard College
c/o Office for Sponsored Research
Holyoke Center, Room 458
1350 Massachusetts Avenue
Cambridge, Massachusetts 02138

James G. Anderson, Principal Investigator
Division of Engineering and Applied Sciences and
Department of Chemistry and Chemical Biology
Harvard University
12 Oxford Street
Cambridge, MA 02138

July 23, 1999

NASA Langley Agreement NAG-1-1305, July 1, 1991–December 31, 1998, "High-Altitude Aircraft and Balloon-Borne Observations of OH, HO_2, ClO, BrO, NO_2, $ClONO_2$, ClOOCl, H_2O, and O_3 in Earth's Stratosphere"

Following is a discussion of developments in our understanding that have emerged from research done under the above-referenced funding.

Development #1: *Determination of the Dominant Catalytic Cycles that Destroy Ozone in the Lower Stratosphere.*

The addition of the newly developed Laser Induced Fluorescence (LIF) instrument to the ER-2 instrument array for the detection of OH and HO_2 at the sub-pptv level provided direct determination of each of the proposed rate limiting radicals in the catalytic destruction of ozone in conjunction with the existing observations of ClO, BrO, NO [Fahey *et al.*, 1993] and NO_2 [Fahey *et al.*, 1989, and Webster *et al.*, 1994a,b]. These observations demonstrated in a series of some fifty flights extending from the arctic to the antarctic vortex that, rather than a catalytic destruction of ozone controlled by nitrogen radicals, the loss of ozone was dominated by hydrogen and halogen loss in the lower stratosphere. Only about 20% of the catalytic destruction rate of ozone results from NO_2 in the lower stratosphere. This is summarized in Figure 1 from Wennberg *et al.* [1994].

The implications of this inversion in the hierarchy of catalytic cycles is critical for the interpretation of the response of the stratosphere to a wide variety of changes, ranging from the injection of volcanic debris, to increasing chorine and bromine loading, to the use of subsonic and supersonic aircraft. Most notably, in a lower stratosphere in which the dominant loss of ozone is dictated by the rate limiting step:

$$NO_2 + O(^3P) \rightarrow NO + O_2$$

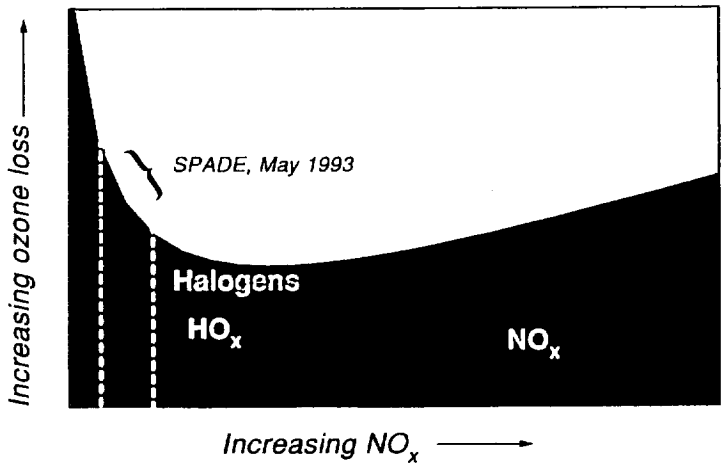

Figure 1. The O_3 removal rate is shown *versus* $[NO_x]$. Because of the coupling that exists between the radical families, the response of the total O_3 removal rate to changes in $[NO_x]$ is highly nonlinear. At sufficiently low $[NO_x]$, such as observed during the NASA mission, the removal rates are inversely correlated with $[NO_x]$.

the addition of halogens would be of minor quantitative importance to the ozone distribution whereas the addition of combustion products, specifically NO_x, from a fleet of aircraft flying in the stratosphere (subsonic or supersonic) would lead to a decrease in

the concentration of lower stratospheric ozone. With the proper partitioning of loss rates among the catalytic cycles defined by direct observation of HO_x, ClO_x, BrO_x, and NO_x, two critical facts emerge.

First, increases in the concentration of any one of the rate limiting radicals would contribute to the total removal rate of ozone by a factor diluted by an amount commensurate with the fractional contribution of the corresponding catalytic cycle to the total. Second, and more important, the *coupling reactions* that link the rate limiting radicals chemically, serve to invert the sign of the response of ozone loss rates to the ensemble of chemical reactions. Both of these features are represented in Figure 1. Specifically, for a fixed NO_x loading, the fractional removal of ozone by each of the families is represented by the vertical segment subsumed by each—the halogens, HO_x and NO_x. The *response* of ozone loss rates to changes in NO_x loading is given by the slope of the sum of the cycles at a given NO_x loading. Since the dominant rate limiting radicals react with members of other catalytically active chemical families(for example, $ClO + NO_2 \rightarrow ClONO_2$, $OH + NO_2 \rightarrow HONO_2$, and $HO_2 + NO \rightarrow OH + NO_2$) the sign of the ozone loss rate resulting from the aggregate of the catalytic cycles inverts with respect to increasing NO_x. This is a development of central importance to the design of the next generation of commercial aircraft and to the public policy debate associated therewith.

Development #2: *The Partial Derivatives of the Rate Limiting Steps are Observables in the Lower Stratosphere.*

Clarification of the fact that the *response* of the ozone concentration in the lower stratosphere to a specific change in concentration (whether it be NO_x loading, aerosol surface area, chlorine, bromine, water vapor, etc.) depends directly on these partial derivatives, not only showed how specific hypotheses could be directly tested by *in situ* observations, it also suggested a research strategy. This is shown explicitly in Figure 2 from Stimpfle *et al.* [1994], which displays the partial derivative of the chlorine rate limiting radical ClO as a function of the NO_2 concentration, all other variables held constant. The relationship of these direct observations to Figure 1 is also indicated.

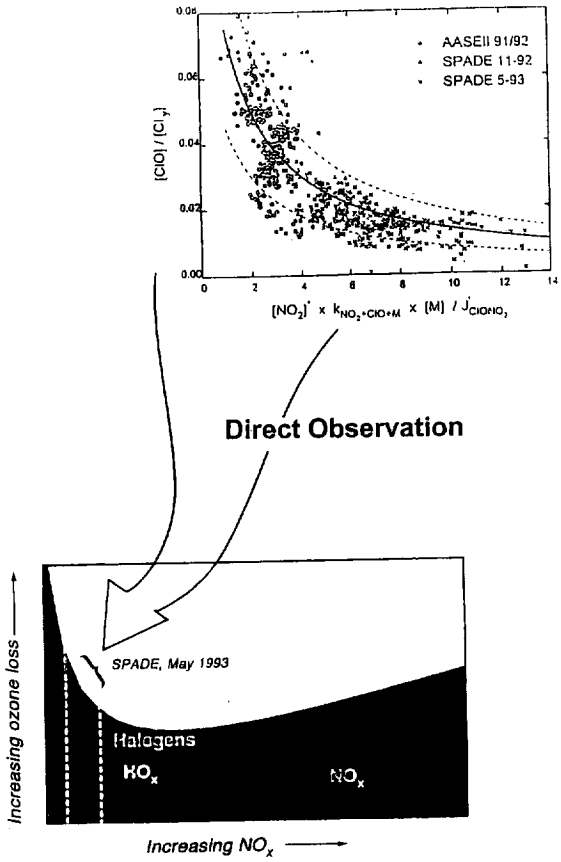

Figure 2. Schematic illustration of the ozone loss rate as a function of the NO_x concentration. Because of the coupling that exists between the radical families, the response of the total ozone loss rate to changes in NO_x is nonlinear. For example, at the low NO_x concentrations, the ozone loss rate was found to be inversely correlated with NO_x. Also shown are actual data obtained by the NASA ER-2 in the stratosphere, which demonstrates that the specific slope of ozone loss is directly observable.

Development #3: *Recognition that the "Low NO_x" Condition is the Regime That Holds the Greatest Potential for Misjudgment of Ozone Loss Rates.*

Inspection of Figure 2 reveals the extremely nonlinear nature of the dependence of ClO concentration on NO_x loading. This is most acute at low NO_x, where ClO increases extremely rapidly for very small incremental decreases in NO_2. This titration behavior is of course reminiscent of the conditions leading to the dramatic loss of ozone over the Antarctic, a condition triggered by low temperatures. However, the observations in Figure 2 were obtained at mid latitudes where the large dynamic range in NO_2 was driven by changes in aerosol reactive surface area as the Mt. Pinatubo debris faded from the lower stratosphere through the course of the last four years. This underscores the highly coupled nature of the system and the many mechanisms that can trigger the removal of NO and NO_2 from the lower stratosphere—increased water vapor, increased aerosol surface area, decreased temperature, etc. This is a particularly important point for assessment models that use mean field temperatures to deduce column ozone loss. The sensitivity of ozone loss to low NO_x conditions means that any *averaging* of temperatures will strongly suppress those conditions for which the maximum opportunity for misjudgment resides. It is perhaps a demonic character of the heterogeneous processes in the lower stratosphere that invariably the products of those highly temperature dependent processes leave (1) the

nitrogen compounds entombed in the solid or liquid phase and (2) the easily photolyzed halogen compounds free in the gas phase.

Development #4: *Mapping of the Bromine Radical Contribution to the Ozone Destruction Rate in the Lower Stratosphere.*

Observations of the BrO concentration from the ER-2 during 1994–96 extended these measurements from the edge of the arctic vortex to the edge of the antarctic vortex with simultaneous observations of ClO and HO_2. This provided the key data to map the halogen rate limiting steps in the lower stratosphere as a function of latitude. Those results are shown in Figure 3.

The outstanding feature of those data is that they demonstrate that bromine is involved in approximately 60% of the total halogen catalytic loss rate of ozone in the lower stratosphere. This conclusion carries important implications. It implies, in combination with the "low NO_x" result, that the predicted recovery of ozone in the next century is not simply related to secular trends in chlorine but rather to the sum of chlorine and bromine, the reactive surface area of aerosols, the partial pressure of water vapor, the nitrate loading, etc. These observations, in conjunction with knowledge of the organic and inorganic bromine reservoirs, defines the relative per-atom efficiency for ozone destruction by bromine with respect to chlorine. Specifically, we show below that bromine is 60–80 times as effective for catalytic destruction per atom.

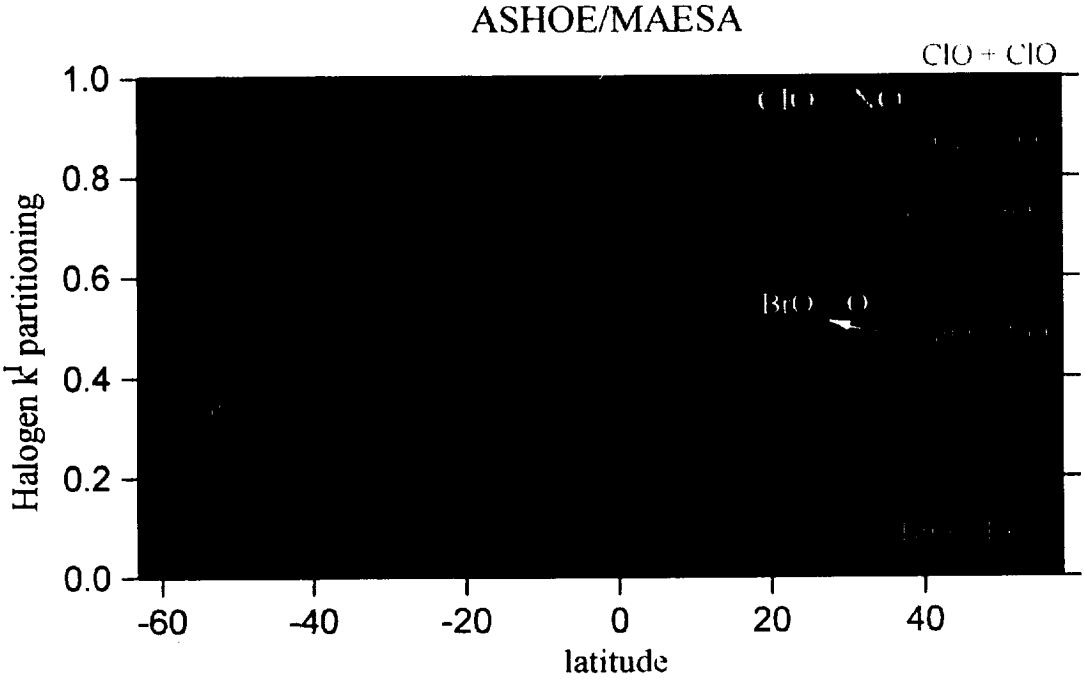

Figure 3. The meridional cross section of the individual rate limiting steps in the halogen system determined from direct observation in the lower stratosphere by ER-2 flights during 1994–96.

Development #5: *Observation of OH, HO_2 and ClO in the Plume of the Concorde SST in the Stratosphere.*

The planned intersection of the ER-2 aircraft with the Air France Concorde over Christchurch, New Zealand, provided high resolution observations of the hydrogen radicals OH and HO_2 under operating conditions for that aircraft in the stratosphere. The observations showed that the oxidation of sulfur in these plumes cannot result from the

gas phase reaction of SO_2 with OH; the observed levels of OH can only be responsible for oxidizing a small fraction (2%) of the SO_2. This is important because the observation of a large number of particles in the aircraft wake [Fahey *et al.*, 1995a,b] require an understanding of the mechanism for particle formation. The existence of such a large number of particles is critical because these aircraft may serve as a means for increasing the aerosol reactive surface area, thereby decreasing the NO_x loading of the stratosphere.

Figure 4 [Hanisco *et al.*, 1997] traces the OH and HO_2 concentrations in three sequential plume crossings and a crossing of the ER-2 wake for comparison.

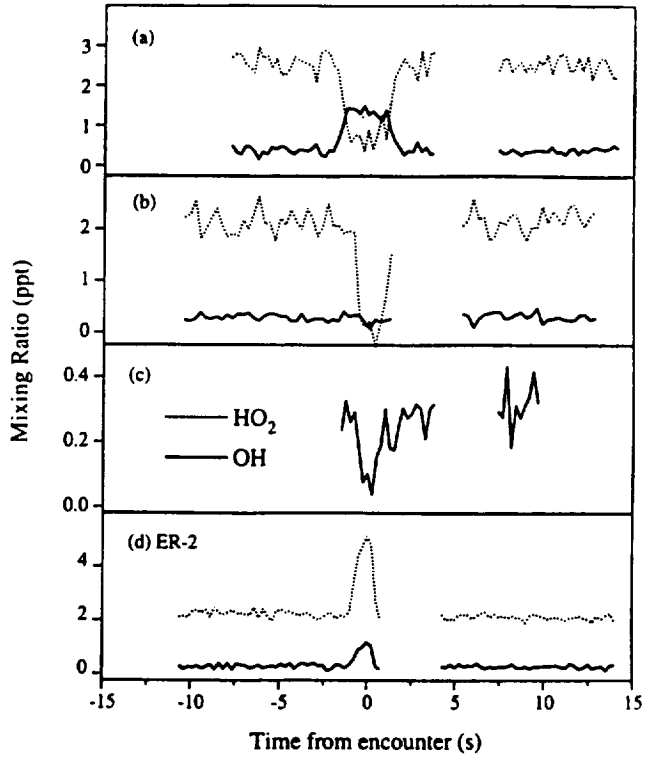

Figure 4. OH (solid line) and HO_2 (broken line) mixing ratios measured during three crossings of the Concorde exhaust plume (a–c) and the single encounter with the ER-2 plume (d). The gaps in the data occur during background calibration of the OH fluorescence signal and (in panel c) during a calibration of the chemical titration of HO_2 [Wennberg *et al.*, 1994b]. The plume ages are (a) 16, (b) 60, and (c) 66 minutes for the Concorde exhaust and (d) 10 minutes for the ER-2 exhaust. Meteorological conditions are: altitude 16.2 km, temperature 222 K, and pressure 100 mb. The Concorde plumes correspond to encounters 3, 9, and 11 observed by the NO_y instrument [Fahey *et al.*, 1995a].

These time-resolved observations were used in a photochemical model that included HONO as the short term reservoir for HO_x and a net loss rate for HO_x driven by $HONO_2$ formation. The reaction mechanism is summarized in Table 1 and the comparison between observed and calculated OH is shown in Figure 5. Based on the ratio of $[HONO]_0/[NO_y]_0$, we estimate the emission index of HO_x to be 0.35±0.17 g OH/kg fuel for the ER-2 encounter with the Concorde operating in the stratosphere at Mach 2. Measurements of a number of volatile particles, thought to be composed of largely of sulfuric acid, implying that at least 12–45% of fuel sulfur is oxidized to H_2SO_4 [Fahey *et al.*, 1995a]. These measurements of HO_x suggest that only about 2% of SO_2 is oxidized by OH via gas phase reactions in the plume.

Table 1. Calculated production and loss rates of OH for encounter #3 (Fig. 4a). Only the most important rates are shown. Rates are in 10^3 molecules/cm^{3}s. Values in parentheses are the percent contribution to the total rate.

	Background Rate		Plume Rate	
		OH Production		
$HNO_3 + h\nu$	3.5	(26)	4.6	(0)
$H_2CO + h\nu$	3.5	(26)	9.9	(2)
$O(^1D) + H_2O$	2.9	(22)	3.3	(1)
$HONO + h\nu$	1.3	(10)	J_{HONO}[HONO]	(95)
$HNO_4 + h\nu$	1.1	(8)	9.6	(2)
total	14.0		1500	
		OH Loss		
$OH + HO_2$	3.2	(21)	5	(0)
$OH + NO_2$	2.9	(19)	852	(57)
$OH + HNO_3$	2.8	(19)	14	(1)
$HO_2 + NO_2$	2.2	(14)	39	(3)
OH + NO	1.3	(9)	512	(34)
$OH + HNO_4$	1.2	(8)	32	(2)
total	15.0		1500	

[H_2O], [OH], and [NO] are measured. [NO_2] is the mean of the measured and calculated steady-state concentrations. [HNO_3] is inferred from the NO_y measurement. [H_2CO], [HNO_4], [$O(^1D)$], and background [HONO] are calculated from steady-state relations. [HONO] in the plume is calculated as described in Hanisco *et al.* [1997].

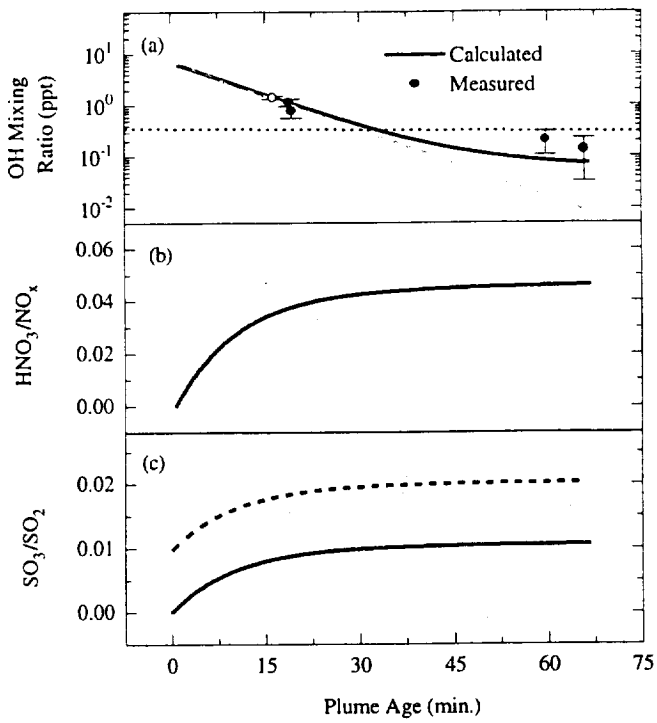

Figure 5. (a) Time evolution of OH produced from HONO photolysis in the Concorde plume. The five measurements (circles) are scaled to $[NO_y]$ in each encounter. The error bars are the 2-σ uncertainties of the measurements. The open circle represents encounter #3. The solid line is the result of the integrating model and the dashed line is the result of Eq. 4, each using $[HONO]_0/[HO_y]_0 = 0.045$. The dotted line corresponds to the 0.3 ppt background level of OH. Oxidation of (b) $NO_2 \rightarrow HNO_3$ and (c) $SO_2 \rightarrow SO_3$ in the plume is shown *versus* plume age. The oxidation ratio is the ratio of emitted NO_x or SO_2 that is oxidized by emitted OH to the total NO_x or SO_2 emitted from the engine. The shaded region includes the 1-σ uncertainty of the calculation. The dashed line in (c) represents the oxidation ratio of SO_2 assuming all HO_x is emitted as OH, the solid line represents the ratio if OH is converted to HONO prior to emission.

These plume crossings represent clear progress in the following areas:

- The practical nature of successfully vectoring the ER-2 into confluence with the wake of an aircraft operating at much higher velocity in the stratosphere has been established. So has the ability to cross the wake multiple times.
- The ability to cross the wake at defined time intervals provides the wherewithal to carry out accurate kinetics within the aircraft wake.
- Normalization to CO_2 concentrations and H_2O concentrations within the wake allows accurate determination of the emission indexes of specific species.
- The high sensitivity and high time response of the HO_x instrument provides unequivocal analysis of the hydrogen radical chemistry in the plume of a supersonic aircraft operating in the stratosphere.
- The observed concentrations of HO_x, NO_x, NO_y, etc., in large measure mimic the results obtained from ground level tests of those engines.

The very large number of particles emitted by the engines, in conjunction with our understanding of the link between aerosol reactive surface and radical partitioning, profoundly changes our view of the relative roles played by the effluents of high altitude aircraft. Specifically, since NO_x is the primary *buffering* agent in the lower stratosphere rather than the primary *catalytic* agent and the lower stratosphere is extremely sensitive to

aerosol loading, the direct impact of NO_x emission is moderated but the concern over changes induced by heterogeneous processes is amplified.

Development #6: *Determination of the Diurnal Behavior of OH in the Lower Stratosphere.*

A remarkable and largely unexpected result that emerged from the extensive ASHOE flights was the simplicity of the relationship between the OH concentration and the solar zenith angle. Results of flights extending from 60°N to 60°S are captured in Figure 6.

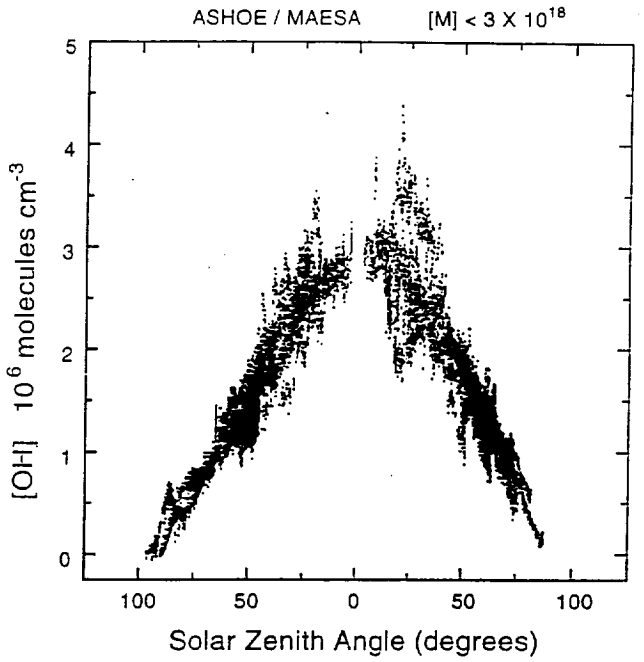

Figure 6. Correlation of [OH] concentration and solar zenith angle from 60°N to 60°S in the lower stratosphere.

What is remarkable is the tight correlation shown in Figure 6 for flights encompassing a large dynamic range in the concentrations of O_3, NO, temperature, and tropopause height. Consideration of these results revealed that the tight correlation results from the fact that HO_x is both produced and destroyed through the OH radical and that the intrinsic correlation between O_3 and NO_y in the lower stratosphere links changes in the source and sink terms of OH such that as the rate of production increases so does the rate of destruction. This stability in the relationship between OH and solar zenith angle provides an important simplification in the diagnosis of the mechanisms that govern catalytic loss in the lower stratosphere. From *Development #1* we have established the fact that over 50% of the catalytic destruction rate of ozone is dictated by the single rate limiting step:

$$HO_2 + O_3 \rightarrow OH + O_2 + O_2 \qquad (1)$$

Thus we can write the HO_x contribution to the catalytic loss of ozone as

$$-d[O_3]/dt = 2k_1[O_3][HO_2]$$

But the exchange of OH and HO_2 in this region of the atmosphere is hypothesized to be controlled by three reactions:

$$HO_2 + O_3 \xrightarrow{k_1} OH + O_2 + O_2$$
$$HO_2 + NO \xrightarrow{k_2} OH + NO_2$$
$$OH + O_3 \xrightarrow{k_3} HO_2 + O_2$$

Since the OH concentration is invariant (to first order) we can rewrite the rate limiting step for ozone destruction as

$$-d[O_3]/dt = 2k_3[O_3][OH]\left\{\frac{k_1[O_3]}{k_2[NO]+k_1[O_3]}\right\}.$$

But since the reaction between HO_2 and NO dominates the path through O_3, this relationship predicts that HO_2 concentrations will (to first order) exhibit a simple inverse relationship to the NO concentration.

Direct observations from ASHOE/MAESA confirm this, as shown in Figure 7. Holding all variables constant, except [NO], the HO_2 concentration drops linearly with increasing [NO]. The product of the reaction rate constant and the concentrations of NO and HO_2 as a function of [NO] demonstrate the functional dependence.

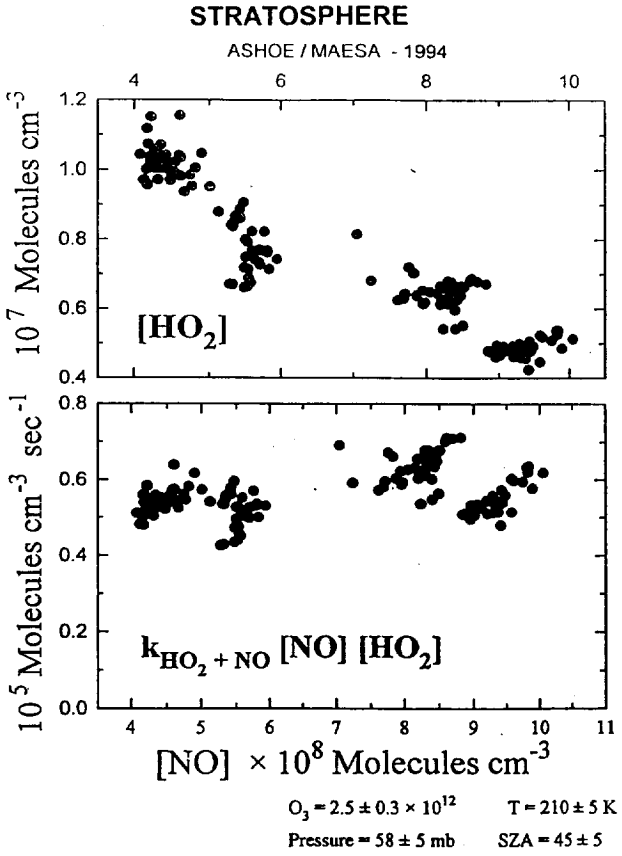

Figure 7. The partial derivative of $[HO_2]$ with respect to [NO] demonstrates the inverse relationship between the rate limiting hydrogen radical and NO_x loading in the lower stratosphere.

Development #7: *Observations of OH and HO_2 in the Troposphere.*

One of the key issues linking atmospheric chemistry, radiation, dynamics and climate is the question of (1) secular trends in upper stratospheric ozone concentrations and (2) the mechanisms that are responsible for the production and removal of ozone in the troposphere and lower stratosphere. The focus on ozone stems both from the fact that ozone is an important greenhouse gas in the upper troposphere (where it is believed to be increasing) and because it is a key agent in the temperature control of the tropopause and lower stratosphere (where it is believed to be decreasing). From a mechanistic point of view, the downward transition from the stratosphere to the troposphere represents, it is hypothesized, the transition from a region characterized by the HO_x catalyzed destruction of ozone to a region characterized by the HOx catalyzed *production* of ozone. As the transition occurs between the stratosphere and the troposphere, the dramatic decrease in ozone concentration and the increase in carbon monoxide concentration leads to a condition in which the exchange between OH and HO_2 is controlled by CO and NO:

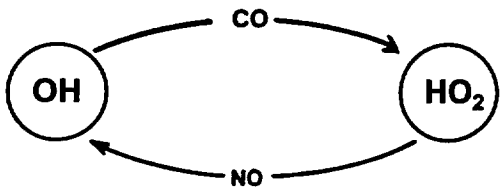

$$\begin{aligned}
&CO + OH \rightarrow H + CO_2 \\
&H + O_2 + M \rightarrow HO_2 + M \\
&HO_2 + NO \rightarrow OH + NO_2 \\
&NO_2 + h\nu \rightarrow NO + O \\
&O + O_2 + M \rightarrow O_3 + M \\
\hline
&CO + 2O_2 \rightarrow CO_2 + O_3
\end{aligned}$$

such that the production rate of ozone is given by

$$d[O_3]/dt = k[CO][OH] = k[NO][HO_2]$$

This underscores the central role that hydrogen radicals play in the photochemical source strength of ozone.

Following the development and test of the LIF ER-2 instrument for detection of OH and HO_2 concentrations, tests were carried out to determine the threshold for HO_x detection in the troposphere and the absence of photochemical interference from species formed in the laser pulse (e.g., the formation of $O(^1D)$ from ozone photolysis followed by reaction with H_2O). "Stairstep" flights and nighttime flights deep into the troposphere were performed. It was demonstrated that the detection threshold for the HO_x instrument in the mid-troposphere is 10 parts per quadrillion (10 parts in 10^{15}), well below expected daytime concentrations. Nighttime flights revealed that the contribution from laser induced formation of OH was well below the detection threshold of 5 parts per quadrillion.

Tropospheric observations of OH and HO_2 were acquired during both the ASHOE/MAESA series and the STRAT flights. An example of 4 Hz data obtained during STRAT in the troposphere at 200 mb is shown in Figure 8. The square-wave modulated signal is displayed in its raw, unfiltered form showing the computer controlled "chop" mode in which the laser is stepped on and off the $Q_1(2)$ rovibronic transition of OH at 282 nm.

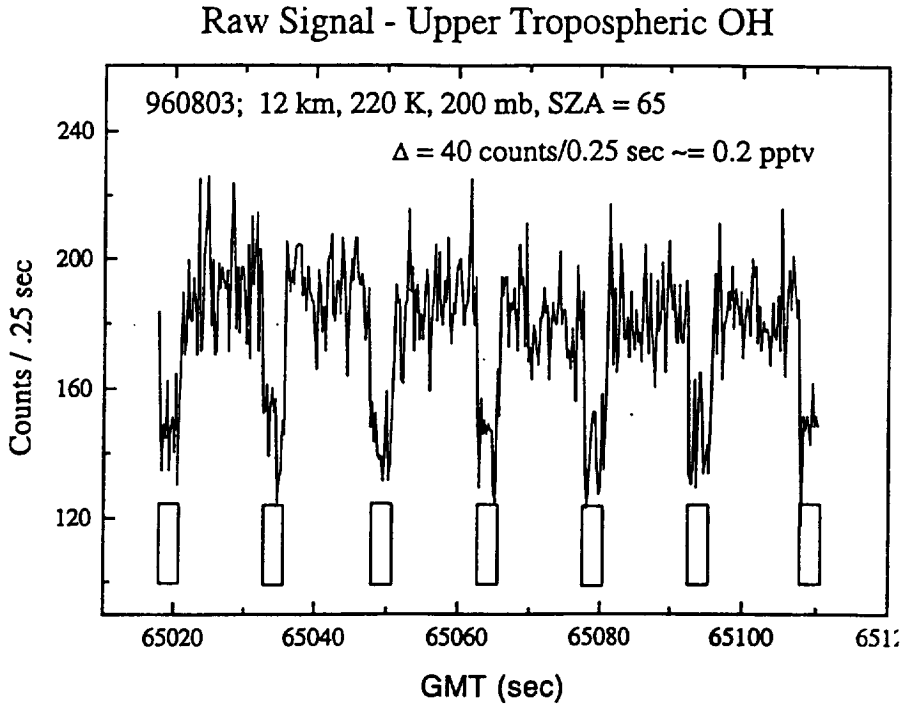

Figure 8. Data obtained during the STRAT mission of OH in the troposphere. The square-wave modulated signal results from the instrument "chop" mode in which the laser is tuned on and off the rovibronic transition at 282 nm.

The concentration of HO_2 is determined by the ER-2 HO_x experiment using the rapid bimolecular reaction

$$HO_2 + NO \rightarrow OH + NO_2$$

to convert HO_2 to OH. The OH is then detected by LIF. This not only yields HO_2 detection limits comparable to those for OH, it also provides extremely accurate measurements of the ratio of HO_2 to OH in the troposphere and lower stratosphere. This ability to determine the OH to HO_2 ratio is a powerful diagnostic tool, as we have demonstrated in the stratosphere (see, for example, Cohen *et al.*, [1994]). When applied to the tropopause and troposphere, it is equally effective. For example, Figure 9 displays the sharp gradient in the HO_2/OH ratio at the tropopause observed by the ER-2 during the ASHOE/MAESA mission. This very large dynamic range over a very limited altitude interval is a powerful technique for testing hypotheses—the establishment of cause and effect within the reaction network as was done in the Antarctic using the gradient across the vortex edge.

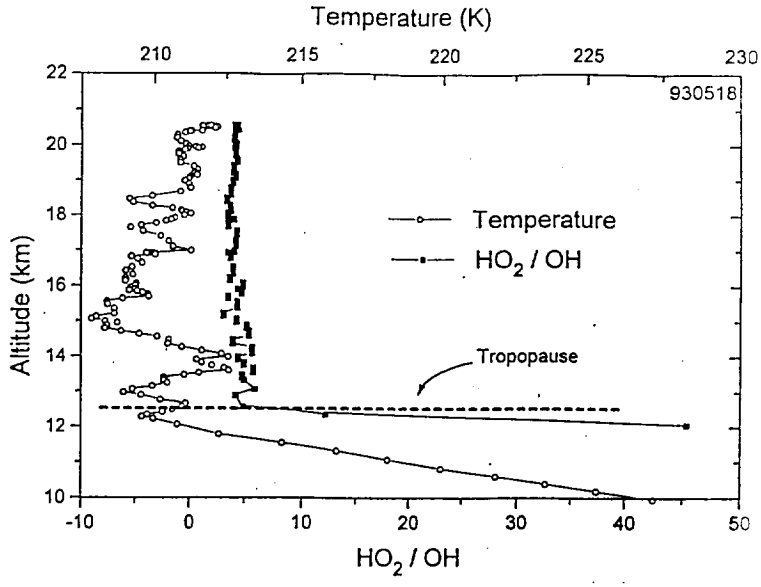

Figure 9. The observed HO_2/OH ratio across the tropopause obtained by the ER-2 during the ASHOE/MAESA campaign.

The ability to detect OH and HO_2 into the lower troposphere provides the opportunity to test the hypothesis that the primary source for the hydroxyl radical in the troposphere is the reaction of $O(^1D)$ plus water. Figure 10 displays the vertical distribution of OH from an altitude of 20 km to an altitude of 6 km. The data points are shown as circles and are compared with the solid line that is the OH concentration calculated using simultaneous observations of O_3, H_2O and UV flux, assuming that OH is produced by the reaction:

$$H_2O + O(^1D) \rightarrow OH + OH$$

It can be seen that between the altitudes of 6–9 km and between 16–20 km, the $O(^1D)$ source adequately explains the observed hydroxyl radical distribution. However, between 9–16 km there is clearly a major discrepancy. The singlet D source fails to explain the OH (and HO_2) concentrations by nearly a factor of three, and in some profiles the discrepancy is even larger.

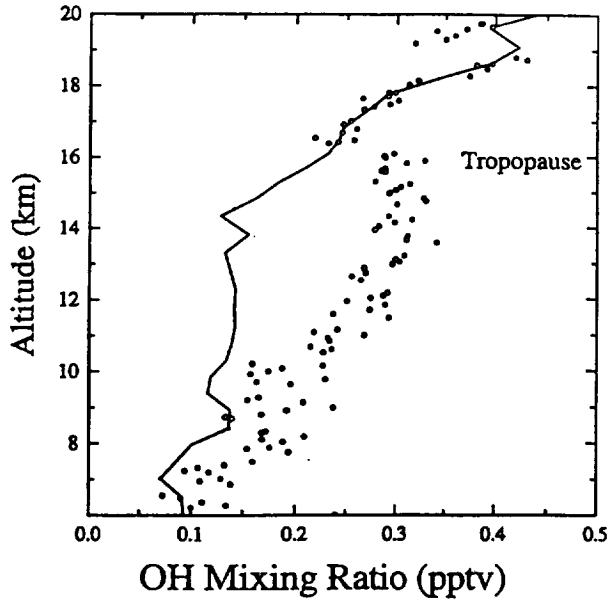

Figure 10. The vertical profile of observed OH in the troposphere superposed on the hydroxyl concentration calculated using $O(^1D) + H_2O$ as the source for HO_x.

The observed departure of OH from the $O(^1D)$ "baseline" is highly variable but is tied to the presence of organic tracers. This has led to the analysis of potential source molecules. Singh *et al.* [1995, 1996] have reported tropospheric observations of acetone in the range 200–400 pptv that are correlated with CO. The photolysis of acetone is a HO_x source [Jaeglé *et al.*, 1997] that will, using the CO-acetone regression of Singh *et al.* in combination with the CO observations of Herman *et al.* [1999] obtained simultaneously with the OH observations, yield a HO_x production rate approaching 10^4 molecules /cc-sec through the mid to upper troposphere. The acetone photolytic source is shown as a function of altitude in Figure 11; the comparison with the singlet *D* source is also shown. These results demonstrate that the source of hydrogen radicals in the troposphere is not as simple as has been assumed prior to the direct observation of OH and HO_2 in the troposphere. There is strong evidence that the source is linked to the presence of organic molecules. There is less direct but plausible evidence that the identity of the source molecule is acetone.

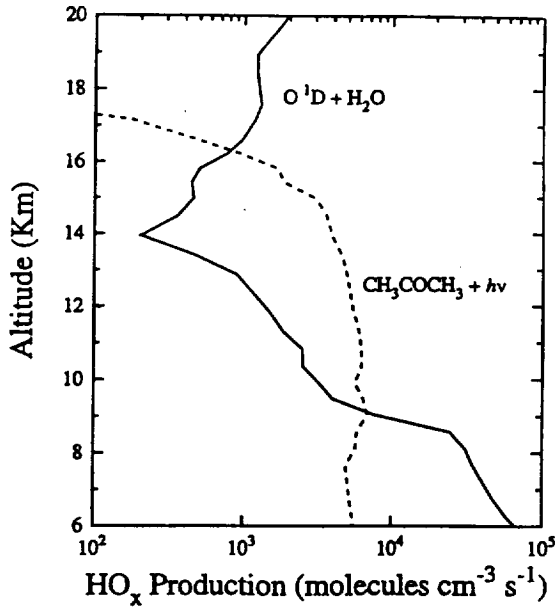

Figure 11. Comparison of the altitude dependence of the HO_x source strength from singlet *D* and from the photodecomposition of acetone.

The demonstration of amplified but variable source terms for HO_x in the troposphere carries important implications for ozone in the troposphere. The enhanced concentrations of OH defined in Figure 11 elevate the photochemical source strength for ozone by an amount approaching 1 ppb/day. This is a critical result, both for the analysis of the mechanism for ozone production in the troposphere and for the analysis of transport processes in this region of the atmosphere.

Development #8: *Analysis of the Catalytic Production of Ozone; Reactions that Couple OH and HO_2 in the Troposphere.*

Stairstep flights executed by the ER-2 in the troposphere and lower stratosphere provide the opportunity, in conjunction with simultaneous observations of OH, HO_2, CO, O_3, and NO, of testing proposed reactions linking the dominant hydrogen radicals and in so doing determining the rate of catalytic ozone production. In the upper troposphere neither the production nor the removal of HO_x is controlled by reactive nitrogen species and the loss rate is determined by both the OH and HO_2 concentrations because the major removal process for HO_x is the bimolecular reaction

$$OH + HO_2 \rightarrow H_2O + O_2 \text{ and by } HO_2 + HO_2 \rightarrow H_2O_2 + O_2 .$$

Given the simultaneous observation of the species listed above, we can track the transition from ozone-nitric oxide control of the OH to HO_2 ratio to carbon monoxide-nitric oxide control in the downward transition from the stratosphere to the troposphere. In Figure 12 we present observations of the fractional contribution of the HO_2 + NO path to OH and of the fractional contribution of the OH + CO path from OH to HO_2 for a stairstep flight from Hawaii during the STRAT mission.

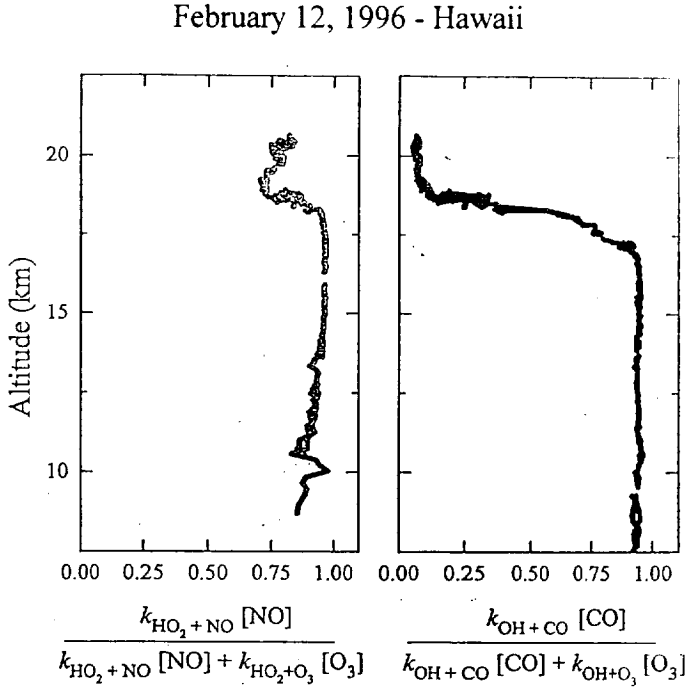

Figure 12. Determination of the dominant exchange reactions linking the OH and HO_2 radicals in the troposphere and lower stratosphere.

Analysis of the dependence of the OH concentration on NO concentration in the troposphere is displayed in Figure 13. This is again a partial derivative in that all

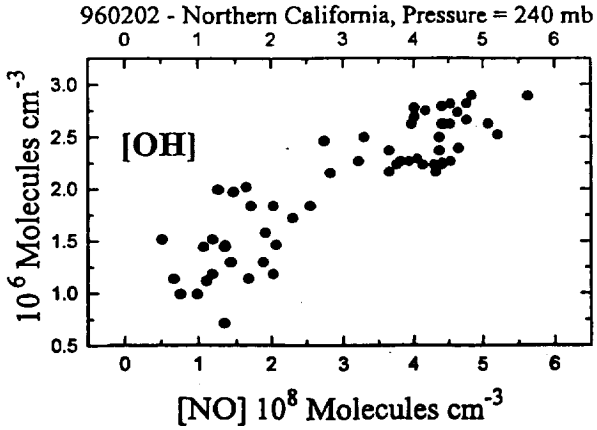

Figure 13. Observed dependence of the OH concentration on the NO concentration in the troposphere.

variables are held constant within a tolerance that balances precision with data volume. The contrast with the stratosphere is striking. Whereas, in the lower stratosphere, the hydroxyl concentration is independent of the nitric oxide concentration, in the troposphere, the OH concentration increases with [NO] reflecting increasing conversion of HO_2 to hydroxyl. The conversion of HO_2 to OH is reflected in the dependence of Perhydroxyl radical concentration on the NO concentration in Figure 14.

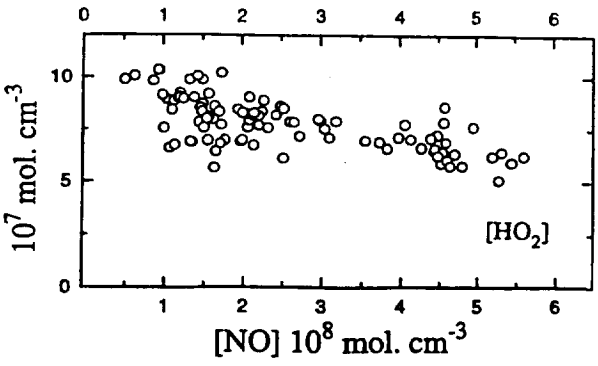

Figure 14. The observed dependence of the HO_2 concentration on [NO] in the troposphere at a pressure altitude of 120 mb.

As noted in the opening of this section, in addition to diagnosing the chemical reaction mechanisms that constitute the reaction network, a key priority of this research is to define the rate of ozone photochemical production in the troposphere. Figure 15 displays the rate of catalytic ozone production from the dominant HO_x cycle—the rate limiting product k_x [HO_2][NO].

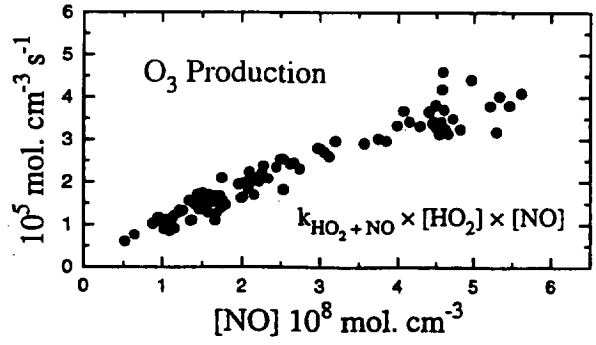

Figure 15. The rate of ozone production in the troposphere based on directly observed concentrations of the rate limiting radicals HO_2 and NO.

Development #9: *Tropopause Temperatures, Water Vapor Mixing Ratios, and Vertical Advection and the Mixing In of Mid-Latitude Air—A developing picture.*

It is generally accepted [Holton *et al.*, 1995, and Newell and Gould-Stewart, 1981] that average tropical tropopause temperatures are too high to explain measured values of q_s, the water vapor mixing ratio in the stratosphere. One can postulate that the reasons for this are either that measurements of mixing ratios are too low, or measurements of tropopause temperatures are too high, or a mechanism for strat-trop exchange occurs preferentially in regions of low tropopause temperatures, or some combination of these. The *in situ* measurements of Kley *et al.* [1979] identifying a water vapor minimum (the hygropause) about 3 km above the local tropopause, and the series of experimental and theoretical papers that presented and analyzed the results of the STEP campaign [1993] observed, identified, and appeared to explain such a mechanism. Accordingly, a period of time existed where "deep convection" into the lower tropical

stratosphere was accepted as the dominant mechanism for air entering the lower tropical stratosphere.

Analysis of *in situ* [Weinstock *et al.*, 1995] and remote [Mote *et al.*, 1995; Mote *et al.*, 1996; Abbas *et al.*, 1996] tropical stratospheric water vapor data as well as correlations of midlatitude carbon dioxide , nitrous oxide, and water vapor measurements [Boering *et al.*, 1997] have shown that the hygropause observed during the summer is not an overshoot but rather is consistent with the seasonal cycle of the tropical tropopause temperature. However, attempts to link the profiles to a vertical transport mechanism through the tropical tropopause has met with limited success. Mote *et al.* [1996] used a transformed Eulerian mean (TEM) 2D trajectory calculation to select latitudes in the tropics where rising air first crosses the 100 hPa-surface. He then uses as a water vapor entry mixing ratio, q_E, determined by the minimum temperature on that surface within each latitude band. These temperature minima are chosen to attempt to compensate for the warm bias found in the United Kingdom Meteorological Office (UKMO) gridded temperatures. Nevertheless, the TEM calculation still yields a maximum q_E value in the summer of 7.5 ppmv, which is inexplicably high.

Carbon dioxide, like water vapor, exhibits a seasonal cycle, albeit slightly out of phase. Because its entry level mixing ratio is independent of entry location and local (thermal) conditions, a model that can relate the measured carbon dioxide mixing ratio profiles in the lower tropical stratosphere to its entry mixing ratios can be used to evaluate the seasonally dependent entry value of water vapor derived from the average thermal characteristics of the "cold trap".

A detailed description of the fast response photofragment hygrometer used in this analysis has been given previously [Weinstock *et al.*, 1994]. Based on detailed laboratory calibrations and in-flight comparison with absorption measurements during ascent and descent its accuracy has been established to be ±10%.

The fast response carbon dioxide instrument is a non dispersive infrared analyzer (Li-Cor Inc. Model 6251) adapted for the ER-2 [Boering *et al.*, 1994], has an accuracy of 0.1 ppmv and a precision of 0.04 ppmv.

CO and CH_4 are measured by the JPL ALIAS diode laser spectrometer [Webster *et al.*, 1994a]. The accuracy of the CH_4 and CO measurements is estimated to be 5%. The OH used in the model calculations is derived from an empirically derived relationship between the OH concentration and the solar zenith angle [Paul Wennberg, Private communication].

All the data presented here were taken on the NASA ER-2 during the Stratospheric Tracers of Atmospheric Transport (STRAT) campaign with missions seasonally timed from the fall of 1995 to the winter of 1996. Tropical profile data were obtained during excursions from cruise altitudes of about 68000 feet to the tropopause and back (hereafter referred to as dives) taken near the southernmost point of southbound survey flights from Barbers Point, HI (22°N). Five of these flights took place during STRAT, on 951105 (yyddmm), 960213, 960801, 060808, and 961211. Water vapor data are available for all these flights, with carbon dioxide data available for all but the 960801 flight. The data presented here are restricted to the dive regions which occur in a latitude region between 2°S and 10°N. The points for all the data sets have been merged into 10-second averages. Figure 16 and 17 present the water vapor and carbon dioxide data, respectively, for the tropical dives, plotted as a function of potential temperature. In each case, the apparent randomness in the shape of the plots is a result of the seasonal cycles of water vapor [Weinstock *et al.*, 1995; Mote *et al.*, 1995] and carbon dioxide [Boering *et al.*, 1995], determined by their respective values as the air rises through the tropical tropopause (the boundary condition) followed by whatever dynamical and photochemical

processes perturb or affect the boundary condition value. For carbon dioxide this boundary condition value, $(CO_2)_{bc}$ can be represented by the average of monthly mean surface CO_2 mixing ratios for Mauna Loa (19°N) and Samoa (14°S) from the NOAA CMDL Flask Network data and delayed by 2 months to match the ER-2 mean CO_2 data for air with $N_2O \approx 310$ ppbv, CO ≈ 30-40 ppbv, and K > 380. [Boering *et al.*, 1997]. The determination of the water vapor boundary condition is one of the goals of this discussion.

It can be shown that the concentration of CO is determined by a balance between its loss from the reaction with OH

$$CO + OH \rightarrow CO_2 + H_2O \qquad (1)$$

and production from the reaction of OH with CH_4

$$OH + CH_4 \rightarrow CO + \text{Products} \qquad (2)$$

where the series of reactions that lead to CO production as summarized by reaction 2 have been presented by Le Texier *et al.* [1988]. For each flight, the transit time for the air represented by each data point is determined by comparing the CO profile measured *versus* potential temperature to one calculated as a function of vertical transit time from the tropical tropopause determined by the rates of reactions 1 and 2. We use an iterative process where for each data set an initial CO mixing ratio of 45 ppbv is used at a tropopause set at 17 kilometers (about 390 K), along with an average CH_4 mixing ratio of 1.7 ppmv valid in the lower tropical stratosphere, and OH concentrations derived from measured solar zenith angles and calculated from a fit of all the STRAT tropical OH data to solar zenith angle. [Paul Wennberg, private communication].

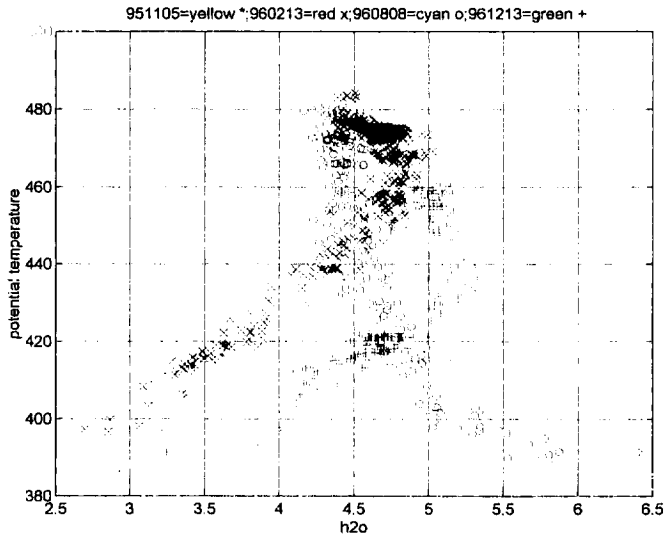

Figure 16. Water vapor data for the tropical dives plotted as a function of potential temperature. Data obtained during the STRAT mission from Barbers Point, HI, on 11/5/95, 11/5/96, 8/8/96, and 12/13/96. The apparent randomness in the profiles is a result of the seasonal cycles of water vapor.

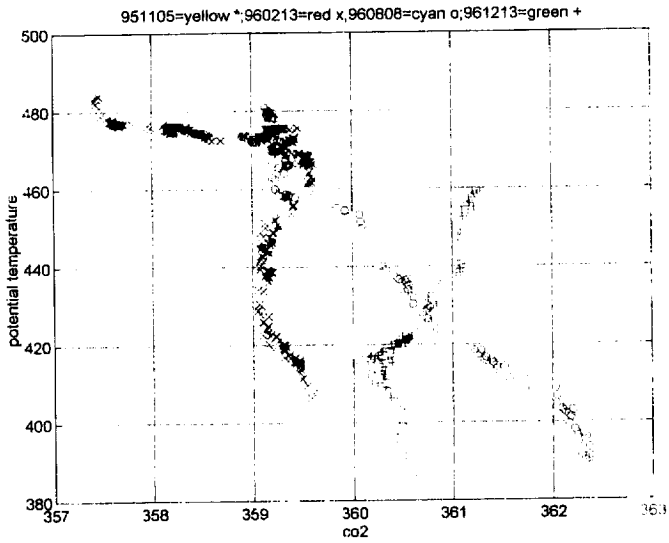

Figure 17. Carbon dioxide data for the tropical dives plotted as a function of potential temperature. Data obtained during the STRAT mission from Barbers Point, HI, on 11/5/95, 12/13/96, 8/8/96, and 12/13/96. The apparent randomness in the profiles is a result of the seasonal cycles of carbon dioxide.

Figures 18 and 19 plot water vapor and carbon dioxide data against the date the air mass crossed the tropopause referenced to January 1, 1996, for all four flights. The boundary condition values for CO_2 and H_2O are included as well. For each flight, data points sampling air encountered closest to the tropopause, which is air that has spent the shortest amount of time in the stratosphere (youngest air), are at the right. The leftmost data points for each flight are the "oldest" and have had the most opportunity for mid-latitude character. Based on this comparison, we demonstrate that water vapor saturation mixing ratios derived from monthly average of radiosonde temperatures between 10°S and 10°N at the tropopause provide an acceptable representation of the boundary condition for water vapor at the tropical tropopause and no special dehydration need be invoked. The 951105 flight provides an excellent and possibly unique example of remarkable agreement between the measured CO_2 and H_2O profiles and the respective tropopause values. The profiles correspond to almost half a seasonal cycle of water vapor and carbon dioxide. Additionally, it specifically demonstrates the success of using the photochemical age of CO as a tracer of vertical ascent in the lower tropical stratosphere. This approach can similarly be useful in studies of strat-trop exchange processes in the tropics where carbon monoxide can provide a tool for determining advection rates near the tropical tropopause.

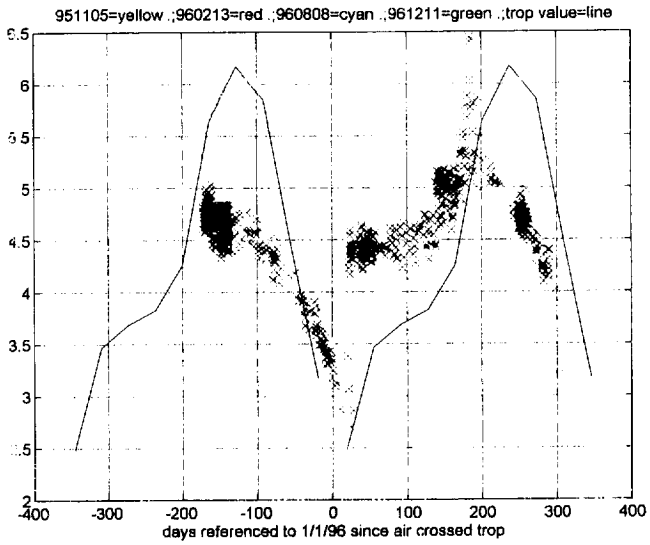

Figure 18. Water vapor plotted against the date the air mass crossed the tropopause, referenced to January 1, 1996, for the flights displayed in Figure 16. The boundary conditions are included as well.

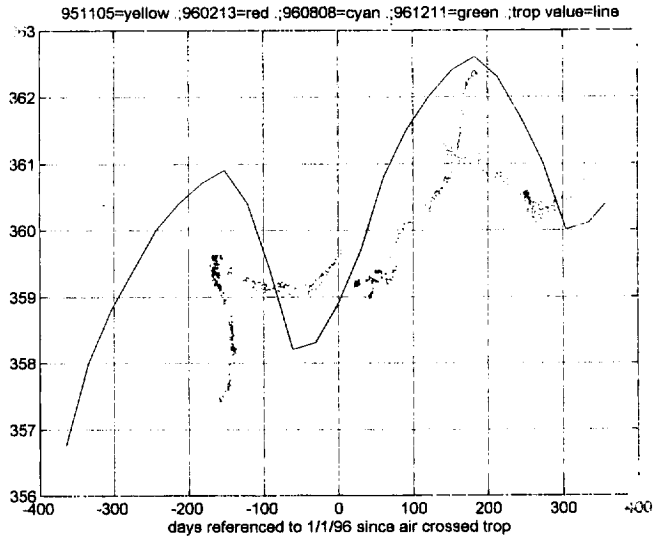

Figure 19. Carbon dioxide plotted against the date the air mass crossed the tropopause, referenced to January 1, 1996, for the flights displayed in Figure 16. The boundary conditions are included as well.

The CO_2 and H_2O profiles from the remaining three flights can be characterized in Figures 18 and 19 as having varying degrees of difference with the reference values. These differences most probably result from the mixing in of midlatitude air. The seasonal and altitude dependence of these mixing processes can uniquely be investigated using these tropical profiles as well as midlatitude water and carbon dioxide profiles measured during STRAT. The fraction of midlatitude air mixed in as well as the altitude dependence of the mixing will impact not only the water and carbon dioxide profiles it

will also affect the calculated photochemical age of the air or ascent time. Accordingly, there is the potential to change the horizontal position as well as the shapes of the profiles in Figures 18 and 19.

Development #10: *Multiple Tracer Analyses as a Diagnostic of Water Vapor Intrusion into the "Middle World".*

During the May 1995 STRAT deployment, the ER-2 flew two stairstep flights with half-hour flight legs in the lowermost stratosphere or middle world. The water vapor measured in the stratosphere near 340–360 K and within a few kilometers of the tropopause exhibited correlations with other tracers very different from what is normally observed in the stratosphere. Observing evidence of transport events in these regions can help us understand the potential impact of aircraft exhaust. Previously, the ER-2 had only sampled these air masses during ascent and descent.

Figure 20 shows a plot of water vapor *versus* N_2O during the 950517 flight, during which a wet air mass extends into the stratosphere, for which the measured N_2O ranges from 290 to 300 ppbv. Figure 21 shows a similar correlation plot for water vapor *versus* CO_2, for which the corresponding CO_2 values extend from 358–360.5 ppmv. In order to help understand the composition of the wet air mass, a simple model is assumed, in which the air mass is taken to be a binary mixture of stratospheric and tropospheric air. The boundary conditions were assumed to be 5 ppmv for stratospheric water vapor, 315 ppbv for stratospheric N_2O and 50–100 ppbv for tropospheric ozone. The CO_2 and H_2O content of the tropospheric air were treated as unknowns. Figure 22 focuses on a linear portion of the water *versus* N_2O plot, which when extrapolated back to 315 ppbv of N_2O, its tropospheric value suggests that the corresponding water content was 25 ppmv. Figure 23 shows the corresponding plot of water vapor *versus* CO_2 with an extrapolated value of 362.5 ppmv for the tropospheric CO_2 content. Figures 24 and 25 provide the similar plots for the 950515 event with the analysis suggesting the tropospheric component contained 360 ppmv of CO_2 and 12 ppmv of H_2O. Based on these CO_2 values, the data are consistent with tropical air entering the stratosphere on 950515 and mid latitude air on 950517.

In both cases, the air could have resulted from mid latitude entry because trajectory analysis shows that tropospheric air near the flight path on 950515 recently came from the tropics. For both flights the mechanism could be isentropic transport across the tropopause because the tropopause was not coincident with theta surfaces. In neither case is there evidence that air with tropospheric character will remain in the stratosphere for more than a month and transport events, as observed here, should not impact the water vapor budget of the stratosphere above 440 K. However, if air with tropospheric character reaches 370–380 K potential temperature surfaces, there is a significant chance for transport into the lower tropical stratosphere, where it can be advected upward and eventually transported poleward into the midlatitude stratosphere.

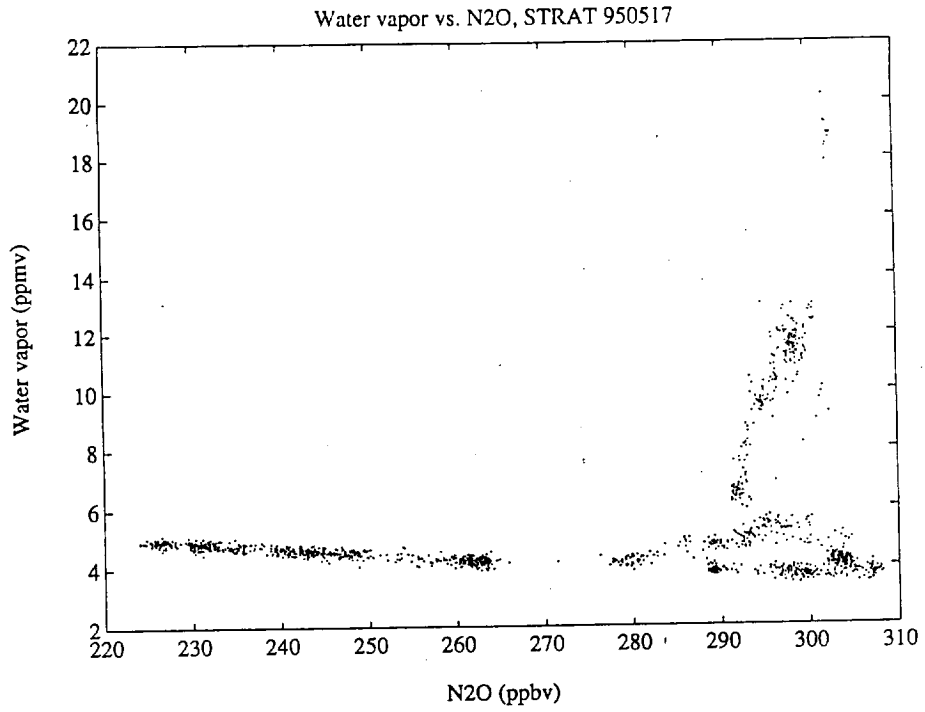

Figure 20. Water vapor *versus* N_2O for the 950517 flight, during which a wet air mass extends into the stratosphere, for which the measured N_2O ranges from 290 to 300 ppbv.

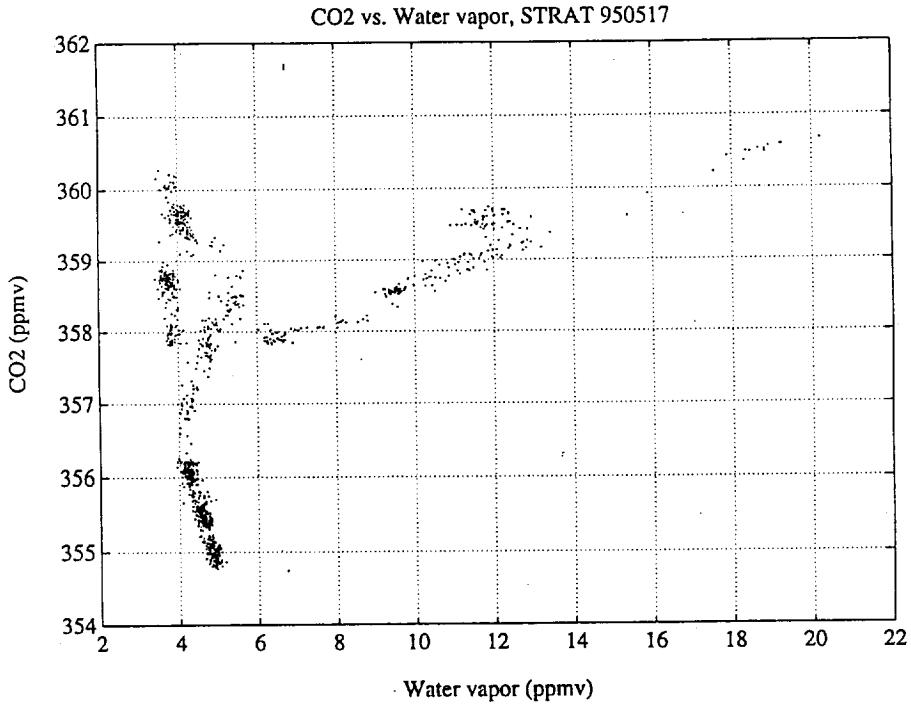

Figure 21. Water vapor *versus* CO_2 from the 950517 flight, for which the corresponding CO_2 values extend from 358 to 360.5 ppmv.

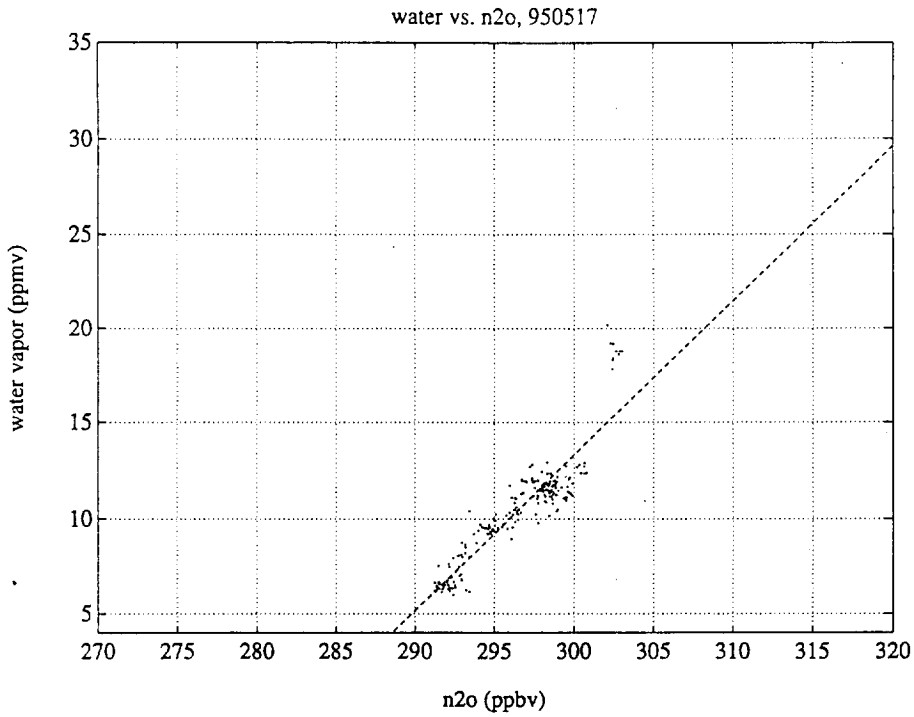

Figure 22. Linear portion of the water vapor *versus* N_2O from the 950517 flight, which provides the data needed to extrapolate back to tropopause values for water vapor of 25 ppmv.

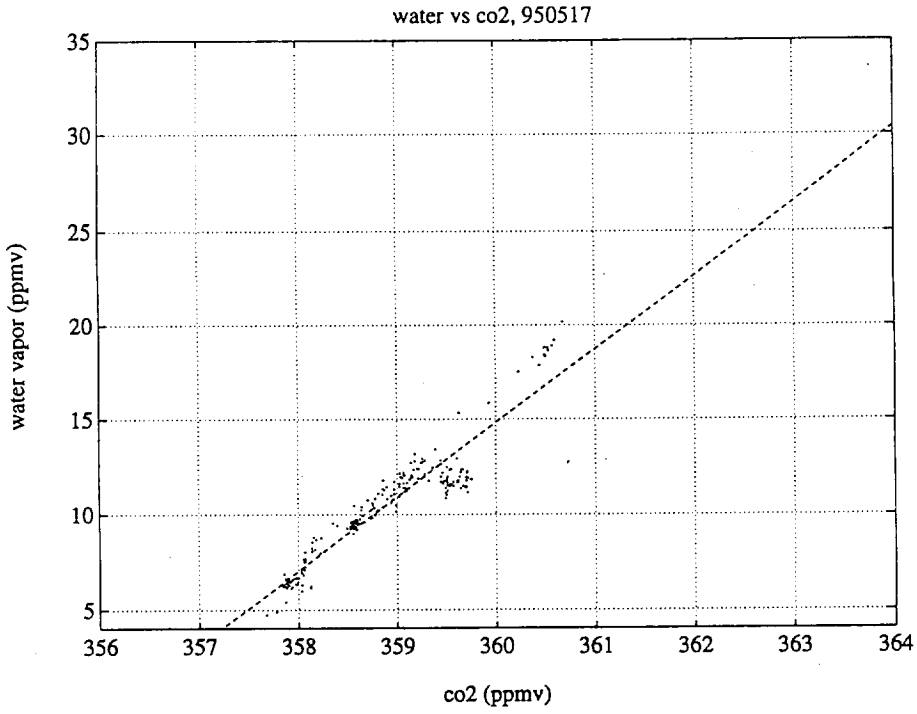

Figure 23. Water vapor *versus* CO_2 from the 950517 flight, with an extrapolated value of 362.5 ppmv for tropospheric CO_2 content.

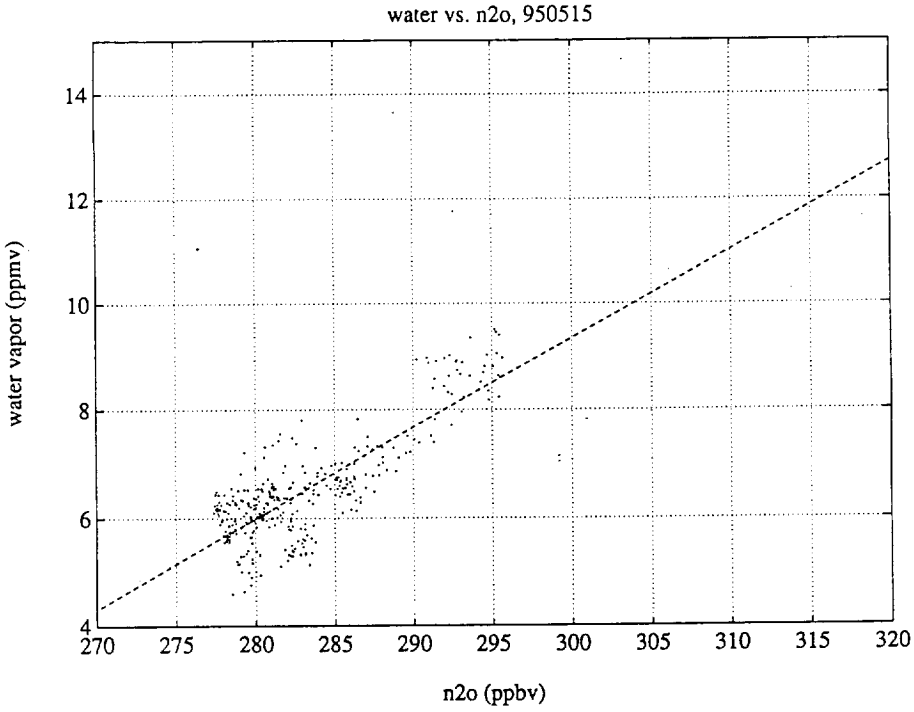

Figure 24. Linear portion of the water vapor *versus* N_2O from the 950517 flight, which provides the data needed to extrapolate back to tropopause values for water vapor of 25 ppmv.

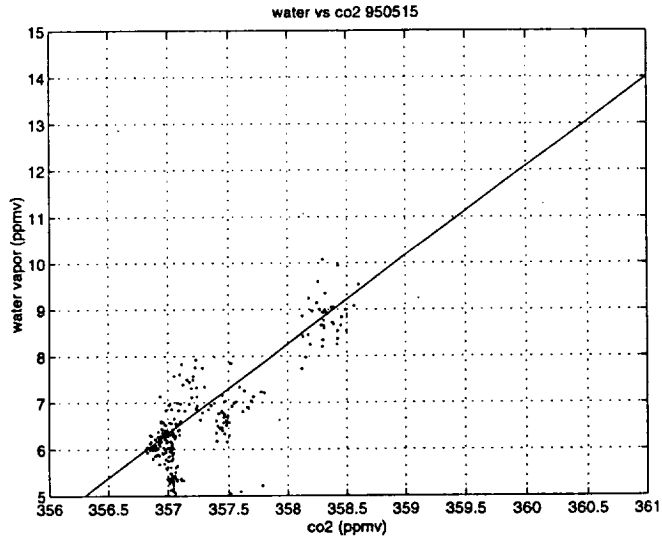

Figure 25. Water vapor *versus* CO_2 from the 950515 flight, with an extrapolated value of 362.6 ppmv for tropospheric CO_2 content.

Development #11: *Flight Testing of a New Instrument for the In Situ Detection of $ClONO_2$ from the ER-2.*

A subset of the most pressing scientific questions in ozone research centers on the chlorine nitrate molecule. For example, does the sum of the HCl and $ClONO_2$

concentrations equal the inorganic chlorine reservoir inferred from observations of the organic and inorganic chlorine species? What is the [ClO]/[Cl_y] ratio under widely varying conditions in the lower stratosphere? How does the $ClONO_2$ concentration depend on the aerosol reactive surface area and on the temperature? What are the initial chlorine nitrate concentrations during the set up of the polar vortex? What is the impact of "reprocessing" on the partitioning of inorganic chlorine in the arctic vortex? What is the temporal evolution of the chlorine nitrate concentration during the recovery phase of the arctic vortex?

In order to answer these questions, we pursued the development of a new flight instrument for the ER-2 that would detect $ClONO_2$, ClO and BrO with the intention of replacing the original ClO-BrO instrument that originally flew on the ER-2 over the Antarctic in 1987. The technique was to employ the thermal decomposition of $ClONO_2$ into products ClO and NO_2 and to detect both of these fragments. We focus on the detection of the ClO fragment in this section, treating the NO_2 product in the section that follows.

The ClO/$ClONO_2$ instrument design must satisfy the following criteria:

- The instrument detection threshold for ClO must be 1 pptv in a 30-second sample; for $ClONO_2$, 10 pptv in a 30-second sample.
- The instrument must detect both ClO and $ClONO_2$ simultaneously.
- The instrument must obtain the measurement of the absolute concentration of both molecules so that, in the course of observation, no destruction of either molecule can take place.
- The instrument must provide scientific demonstration of the observation of absolute ClO and ClONO2 concentrations without loss within the instrument and it must demonstrate this in flight.
- The absolute calibration must be checked in flight.
- All aspects of the flight instrument performance envelope must be directly investigated in laboratory studies prior to and following flight.
- The instrument must be fully computer controlled; it must perform its complete flight protocol with only an "on" command from the cockpit.

The technique selected for the detection of ClO was to use the rapid bimolecular reaction

$$ClO + NO \rightarrow Cl + NO_2$$

to convert ClO to Cl. The Cl product is then detected by atomic resonance scattering (see, Anderson *et al.* [1977], Brune and Anderson [1986], and Brune *et al.* [1989]).

Detection of $ClONO_2$ is executed by the thermal decomposition of the parent molecule by precipitously elevating the temperature of the flowing sample to thermally decompose chlorine nitrate into ClO and NO_2:

$$ClONO_2 \xrightarrow{\Delta} ClO + NO_2$$

The design of the instrument is shown in an exploded schematic in Figure 26.

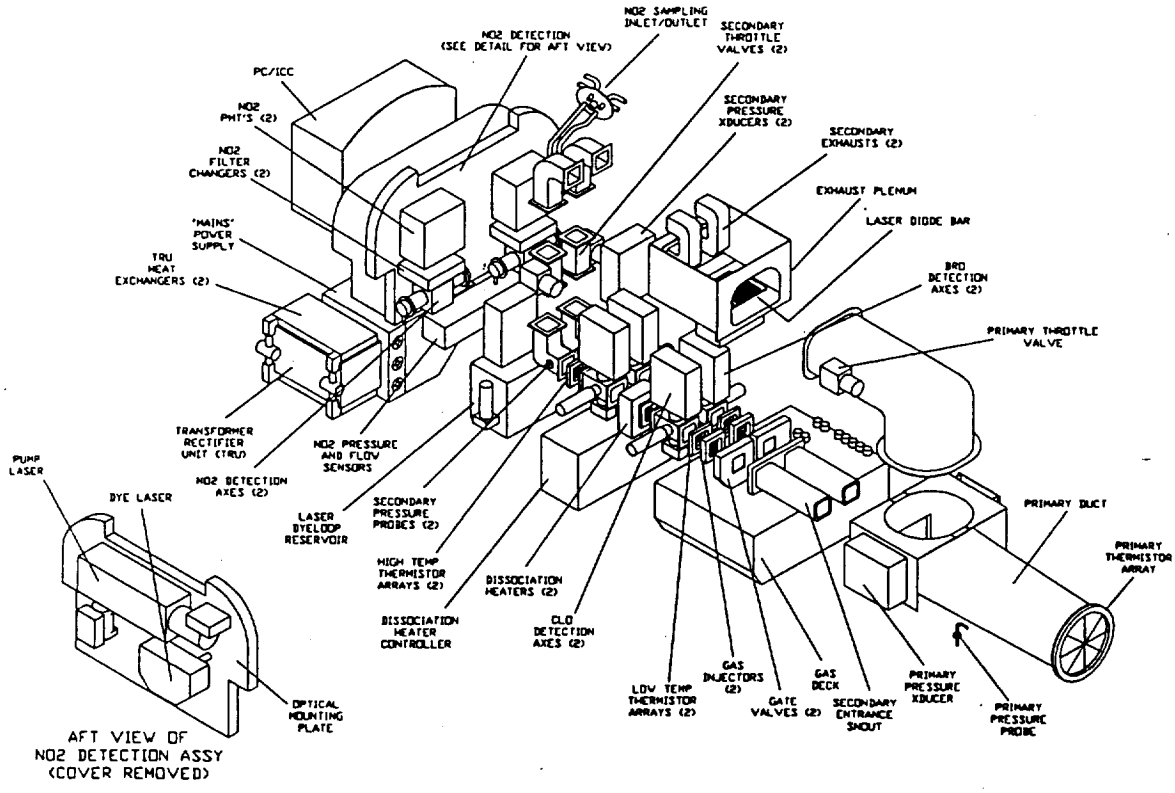

Figure 26. Schematic of the $ClONO_2$, NO_2, ClO, BrO instrument showing the architecture of the duct arrangement, both primary and dual secondary, the location of the detection axes, dissociation heaters, the optical plate that contains the NO_2 laser-induced fluorescence system, gas addition deck computer subsystems, power handling system, throttle valve positions, exhaust plenum, and NO addition systems.

The "primary flow" is extracted from the aircraft free stream by the primary duct from the leading edge of the ER-2 super pod. The duct design minimizes the boundary layer depth, maintains laminar flow in the core of the primary flow, and maintains a symmetric boundary layer within the primary duct. Two secondary ducts extract the laminar core of the primary flow, each maintaining a symmetric boundary layer of minimum depth such that the laminar core of each duct reaches the optical detection axes unperturbed. The first set of optical axes in each duct detect ClO or BrO, following the addition of NO. Flight data demonstrating the Cl yield from ClO as a function of added NO is shown in Figure 27.

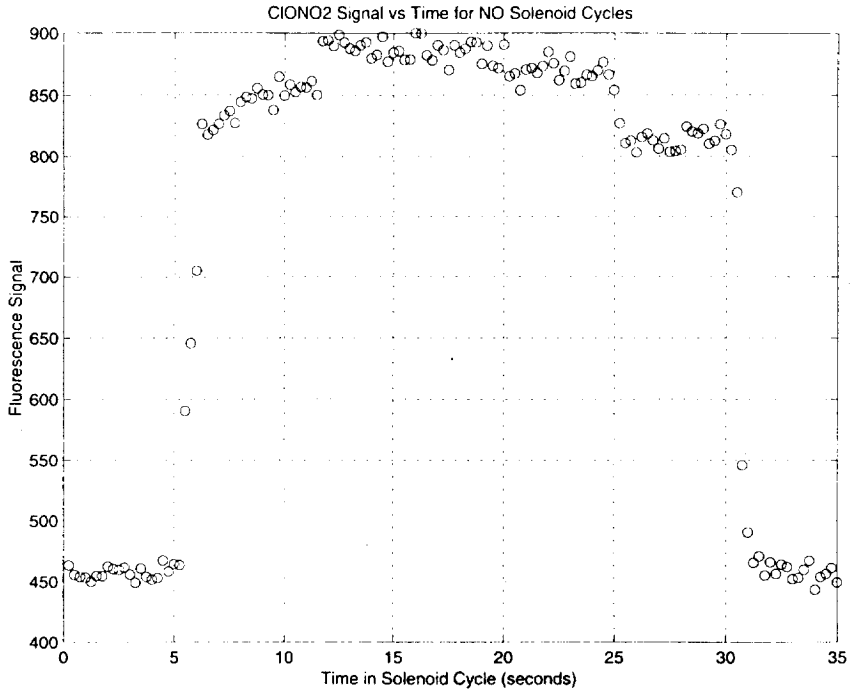

Figure 27. Flight data showing the Cl atom yield from $ClONO_2$ dissociation. The shape of the modulated signal results from the concentration scan of NO added to demonstrate the kinetics of the formation of Cl from ClO formed in the dissociation process. The leading edge of the square wave corresponds to the highest flow rate of NO, the trailing edge corresponds to the lowest flow rate.

Immediately following the first optical axes in each duct is an array of doped Si heating elements that allow the flow temperature to be scanned from ambient to 550 K with high resolution. Considerable effort was invested in the laboratory investigation of this method. The first issue that was investigated was the quantitative yield of ClO from $ClONO_2$ thermal decomposition under conditions of pressure, flow velocity, etc., encountered during flight. Those data are shown in Figure 28. In those experiments, the flight instrument was an integral part of the laboratory flow system, to which a calibrated amount of chlorine nitrate was added. Flow velocity and pressure were controlled such that conditions that were encountered during flight were well within the regime covered in the laboratory experiments.

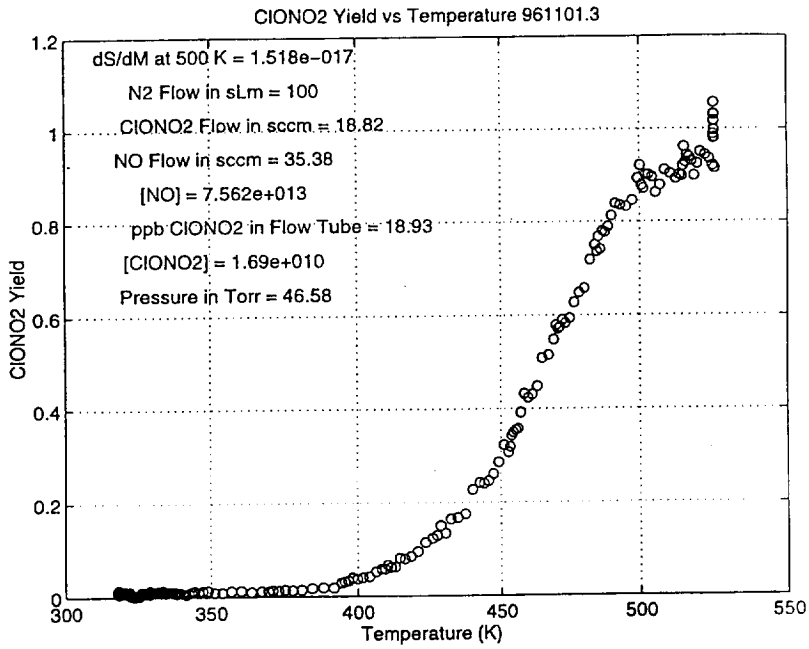

Figure 28. Laboratory data using the flight instrument, showing the temperature dependence of Cl atom yield from ClONO2 dissociation as a function of temperature

The temperature dependence of Cl yield from $ClONO_2$ matches that calculated for simple unimolecular decomposition of chlorine nitrate, demonstrating that the process is executed by simple gas phase collisions. Absolute calibration of the instrument was carried out as a function of temperature. It was discovered that at elevated temperatures of the instrument wall, the instrument sensitivity became a function of the instrument lamp-module/flow-tube-wall temperature caused by the release of gas phase species by the aluminum wall. For this reason, the final flight design included the addition of a cooling manifold that directs forced cold air from the free stream onto the O_2 cell in front of the resonance lamp, onto the O_2 cell in front of the photomultiplier, and onto the region in front of the UV monitor. This drives the operating temperature of the optics to less than 0°C during flight and thereby eliminates any temperature dependence resulting from the instrument itself from the calibration. We determined that the mechanism responsible for the drop in sensitivity above temperatures of 40°C is the vapor pressure of water that absorbs at 119 nm, emitted by the aluminum cell through which O_2 flows. The O_2 cell in front of the lamp exists for the purpose of eliminating all resonance lines in the multiplet of atomic chlorine, except the $^2D_{5/2}$-$^2P_{3/2}$ transition at 118.8 nm.

The instrument flew in its first science mission in the first **P**hotochemistry of **O**zone **L**oss in the **A**rctic **R**egion **I**n **S**ummer (POLARIS) deployment in April-May 1997. Instrument performance was excellent. All subsystems of the instrument operated within design limits: the computer control and data acquisition; the duct throttle valves and gate valves; the array of gas addition systems; the RF oscillator-amplifiers; the detectors; the $ClONO_2$ dissociation heater and heater control systems; and the boundary layer analysis systems. Instrument design characteristics were demonstrated: Optical sensitivity was significantly improved over the ClO instrument that originally flew into the Antarctic in 1987; thermal tailoring proved to be highly effective; optical components

operated in the 0°C range in flight, boundary layer growth was symmetric and minimal; and the extracted ClO and $ClONO_2$ concentrations exhibited no velocity dependence in the range from 5–30 m/sec.

The detection threshold for ClO and $ClONO_2$ proved to be in the 1 pptv range for a 30 second sample, the thermal yield of ClO from $ClONO_2$ matched the laboratory data. Figure 29 shows the temperature scans of the Cl yield from $ClONO_2$, demonstrating the same sigmoidal shape as the laboratory data and the same plateau at elevated temperature, demonstrating the absence of loss processes with increasing temperature above the point of complete dissociation of the parent molecule.

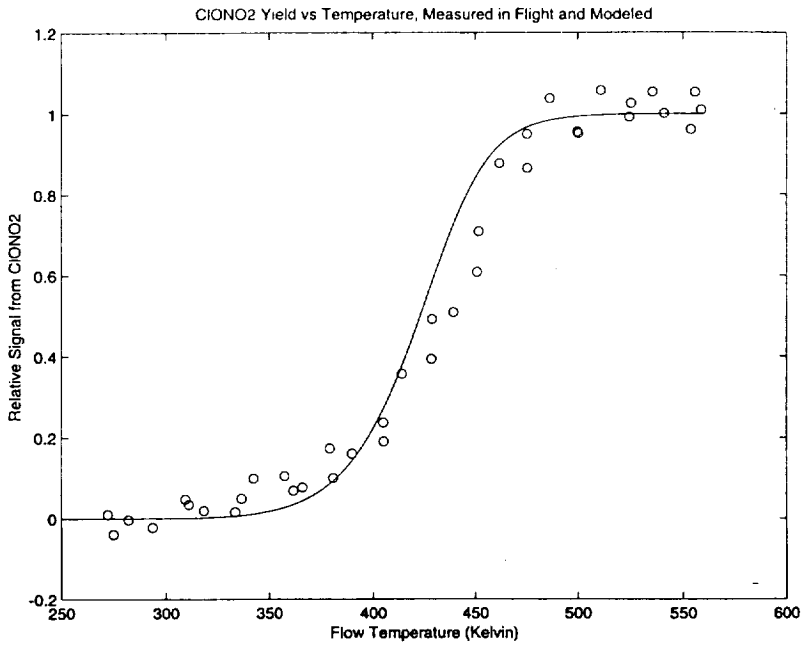

Figure 29. Flight data showing the temperature dependence of the Cl yield from $ClONO_2$ thermal dissociation. The sigmoidal shape of the flight data mimics that of the laboratory data shown in Figure 28.

The yield of Cl (as a function of added NO) from $ClONO_2$ thermal decomposition is also textbook in its behavior. Flight data from the first POLARIS deployment is shown in Figure 30, in combination with the yield curve for Cl atoms plotted *versus* the product of NO concentration and reaction time. The instrument is designed to scan the NO concentration as a function of time, beginning with high NO flow rates (corresponding to [NO] ~ $5 \times 10^{13}/cm^3$) and sequentially dropping in concentration such that the Cl atom yield increases with decreasing [NO] until the peak yield is reached and then decreases with decreasing [NO] conditions, corresponding to conditions of incomplete conversion of ClO to Cl.

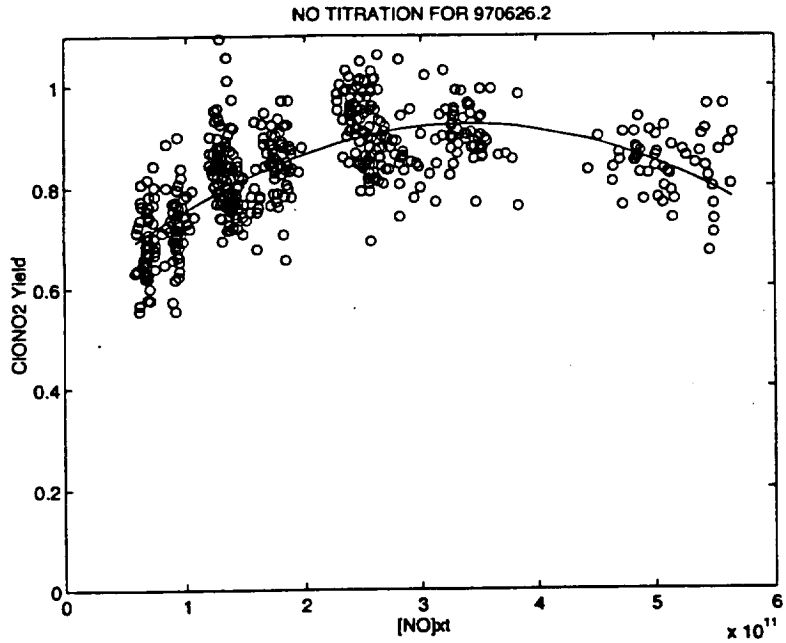

Figure 30. Flight data showing the yield of Cl atoms as a function of the product of [NO] and reaction time, *t*. The variability in the data at a fixed value of [NO] results from the changing concentration of $ClONO_2$ in the atmosphere.

Results from the POLARIS mission are shown in Figure 31, in which the observed chlorine nitrate concentrations are shown for an ER-2 flight north from Fairbanks, Alaska, on June 26, 1997. The structural detail shown in the $ClONO_2$ data is correlated precisely with the ClO data and is anticorrelated with N_2O tracer data. While there is not space here for any in-depth analysis of the flight data and its relation to laboratory data, that analysis has been done and it is clear that the $ClONO_2$ instrument has matched or exceeded its design goals.

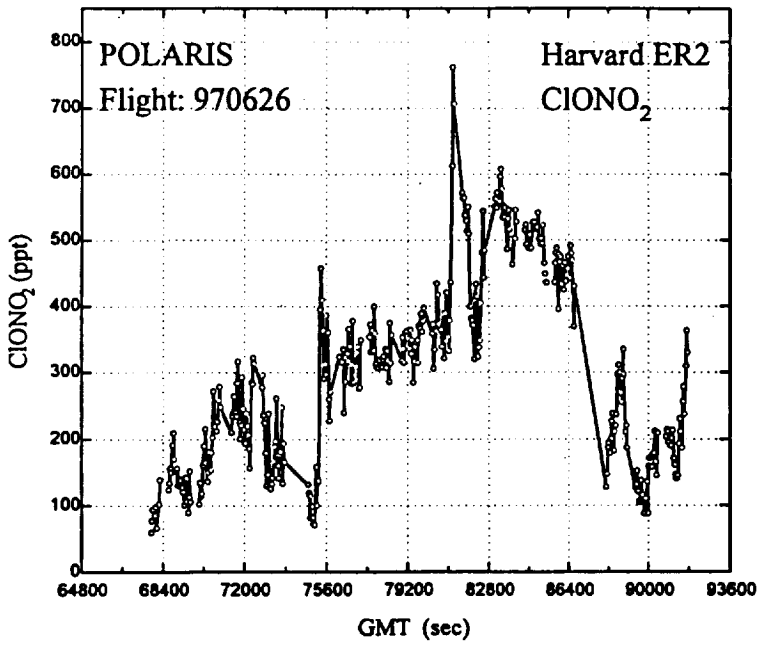

Figure 31. Results from the first POLARIS mission flown from Fairbanks, AK, showing the observed chlorine nitrate concentration as a function of aircraft flight time.

Development #12: *Laser Induced Fluorescence Detection of NO_2.*

Nitrogen dioxide is a critical radical in the current research agenda for several important reasons. First, it occupies the rate-limiting step in the dominant nitrogen catalytic cycle in the Earth's stratosphere. Observation of its concentration is critical for a quantitative appraisal of the rate of ozone destruction resulting from the entire family of reactive nitrogen compounds. Second, it is the primary radical linking the nitrogen species with both the hydrogen radicals and the halogen radicals through the reactions

$$OH + NO_2 + M \rightarrow HONO_2 + M$$

$$ClO + NO_2 + M \rightarrow ClONO_2 + M$$

$$BrO + NO_2 + M \rightarrow BrONO_2 + M$$

It is also the radical responsible for the extraction of the very large ClO concentration responsible for rapid ozone destruction in the winter vortices. Third, it is the recipient of the oxidation of NO by ozone at night and thus is a unique measure of NO_x in the stratosphere and upper troposphere.

From the analytical perspective of *in situ* chlorine nitrate detection in the stratosphere, it is also the companion fragment formed in the thermal decomposition of $ClONO_2$ in the new ER-2 flight instrument:

$$ClONO_2 \xrightarrow{\Delta} ClO + NO_2$$

The central importance of NO_2 to stratosphere/troposphere chemistry, its importance to the detection of $ClONO_2$, and the difficulty of directly detecting the species led to the development of a component of the ER-2 chlorine nitrate instrument dedicated to the LIF detection of this species.

As described under *Development #1*, we have successfully applied LIF to the detection of OH, and we have done the preliminary spectroscopy and optical development of LIF for NO_2 [Larabee, 1984]. We thus pursued the development of the ER-2 flight instrument using the new fiber-optic coupled (FC) laser developed recently by Spectra Physics (Model Z30532Q) as the pump laser in a dye laser system modeled after the HO_x instrument. The 532 nm doubled output from the YAG laser operates at a pulse repetition rate equal to or greater than 5 kHz with an average output of 4 watts, a beam divergence of 3 mrad in TEM 00 mode, with a pulse length of ~30 nsec. The leading edge of the pulse is used to establish oscillation and the remainder of the pulse for amplification such that the tunable output at 585 nm has an average power of 300 mwatts and a repetition rate of >5 kHz. The laser optical system is combined on a single optical plate that is inserted vertically into the $ClONO_2$ flight instrument (see Figure 26). One side of the composite plate contains the solid state laser system, fiber-optic coupling system, dye laser and coupling optics; the other side of the optical plate contains the NO_2 detection, NO_2 flow control and measurement sub-systems, laser flux diodes, etc.

The absolute calibration of the NO_2 LIF system is approached from three perspectives. First, laboratory calibrations are performed with known NO_2 concentrations (taken from a standard compared against the known infrared cross section of NO_2) normalized to the laser flux passing through the optical amplification cell (a multipass White cell). Thus, the NO_2 fluorescence emitted between 700–850 nm is tied to the NO_2 absolute concentration for a given photon flux through the cell. Second, using a computer controlled actuator, the interference filter that selects the NO_2 fluorescence is replaced by a narrow band pass filter that passes only the Raman line of N_2. Thus, in the laboratory

calibration phase, a known NO_2 concentration is introduced into the instrument in flight configuration and the detector count rate resulting from NO_2 fluorescence is determined for a given Raman scattered count rate. The advantage of this technique is that the detection geometry and photomultiplier are identical for both the fluorescence measurement and the Raman normalization. Third, the gas addition deck for the ER-2 flight instrument is equipped with an NO_2 calibration system that can add a known amount of NO_2 to the intake port of the instrument during flight. This provides an on-board source of NO_2 at known concentration that is calibrated against the Raman signal in flight, and against the laboratory standard when the aircraft returns from a flight.

Results from the first POLARIS deployment are shown in Figure 32. The laser is designed to execute a resonance line "seek and look" algorithm to find the line at 585 nm, and then a "chop mode" algorithm that steps on resonance-off resonance to establish the square wave modulation shown in Figure 32 for the calibration cycle. An on-board cell containing NO_2 is used to compare with the *in situ* data.

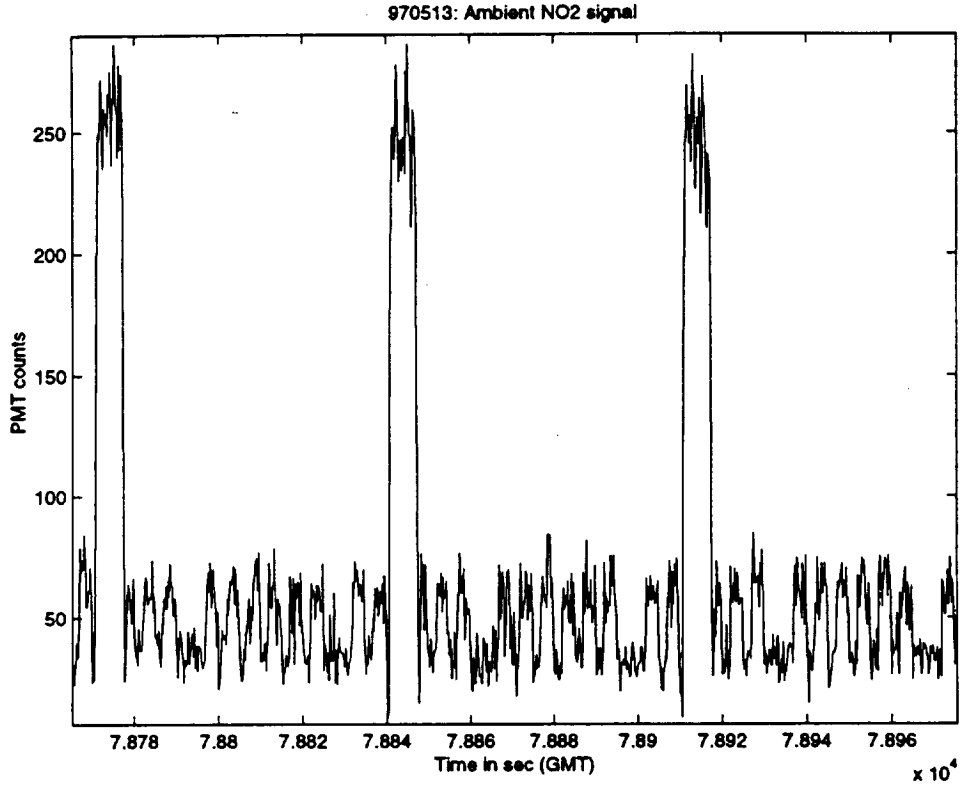

Figure 32. Flight data showing the raw NO_2 data obtained during the computer controlled "chop mode" that steps on and off the 585 nm resonance line of NO_2. Calibration pulses are shown interspersed with the ambient NO_2 signal.

Results of the *in situ* NO_2 observations from the first POLARIS deployment are shown in Figure 33 and are compared against the ozone "tracer" data from the same flight. At the concentration observed during POLARIS, the signal-to-noise of the NO_2 observation is ~100/1 for a 30-second sample.

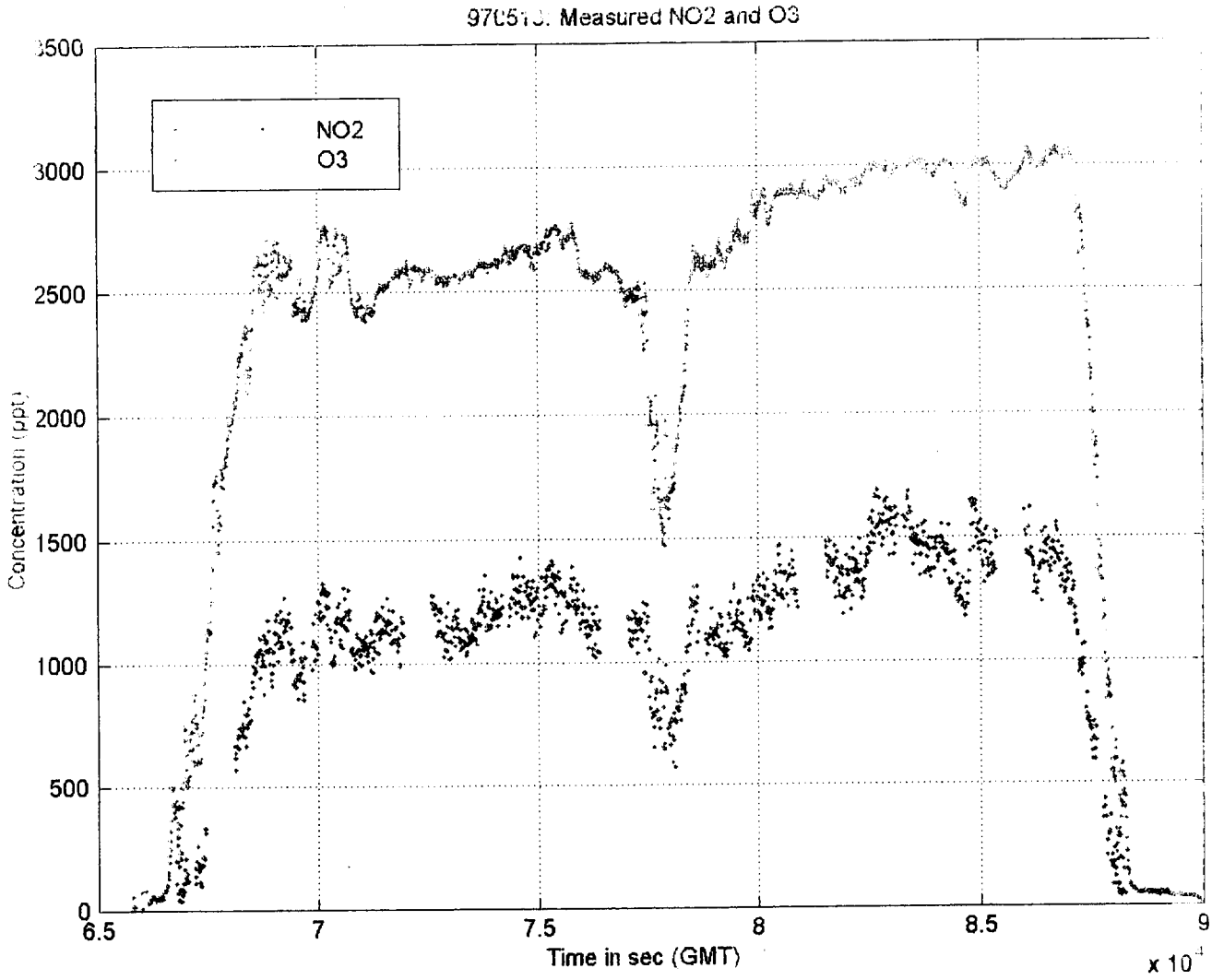

Figure 33. The concentration of NO_2 obtained during the first deployment of the NO_2 LIF system during POLARIS. The NO_2 observations are shown with the ozone concentration simultaneously obtained in the flight.

Thus, a new approach to NO_2 detection has been developed, calibrated, and flight tested. There are currently several advances in detector technology and optical design that will improve the detection threshold such that NO_2 concentrations at the 10 pptv level will be realized in a 30-second sample with excellent signal-to-noise ratios.

REFERENCES

Anderson, J. G., J. J. Margitan, and D. H. Stedman, "Atomic chlorine and the chlorine monoxide radical in the stratosphere: Three *in situ* observations," *Science* **198**, 501–503, 1977.

Abbas, M. M., *et al.*, "Seasonal variations of water vapor in the lower stratosphere inferred from ATMOS/ATLAS-3 measurements of H_2O and CH_4," *Geophys. Res. Lett.* **23**, 2401–2404, 1996.

Boering, K. A., *et al.*, "Tracer-tracer relationships and lower stratospheric dynamics: CO_2 and N_2O correlations during SPADE," *Geophys. Res. Lett.* **21**, 2567–2570, 1994.

Boering, K. A., *et al.*, "Stratospheric mean ages and transport rates form observations of carbon dioxide and nitrous oxide," *Science* **274**, 1340–1343, 1997.

Boering, K. A., *et al.*, "Measurements of stratospheric carbon dioxide and water vapor at northern midlatitudes: Implications for troposphere-to-stratosphere transport," *Geophys. Res. Lett.* **22**, 2737–2740, 1995.

Brune, W. H., and J. G. Anderson, "*In situ* observations of midlatitude stratospheric ClO and BrO," *Geophys. Res. Lett.* **13**, 1391–1394, 1986.

Brune, W. H., J. G. Anderson, and K. R. Chan, "*In situ* observations of ClO in the Antarctic: ER-2 aircraft results from 54°S to 72°S latitude," *J. Geophys. Res.* **94**, 16,649–16,663, 1989.

Cohen, R. C., *et al.*, "Are current models of catalytic removal of ozone by HO_x accurate? New constraints from *in situ* measurements of the OH to HO_2 ratio," *Geophys. Res. Lett.* **21**, 2539–2542, 1994.

Fahey, D. W., *et al.*, "*In situ* measurements of total reactive nitrogen, total water, and aerosol in a polar stratospheric cloud in the Antarctic," *J. Geophys. Res.* **94**, 11299–11315, 1989

Fahey, D. W., *et al.*, "*In situ* measurements constraining the role of sulphate aerosols in mid-latitude ozone depletion," *Nature* **363**, 509, 1993

Fahey, D. W., *et al.*, "Emission measurements of the Concorde supersonic aircraft in the lower stratosphere," *Science* **270**, 70-74, 1995a.

Fahey, D. W., *et al.*, "*In situ* observations of aircraft exhaust plumes in the lower stratosphere at midlatitudes," *J. Geophys. Res.* **100**, 3065-3074, 1995b.

Hanisco, T. F., *et al.*, "The role of HO_x in super- and subsonic aircraft exhaust plumes," *Geophys. Res. Lett.* **24**, 65-68, 1997.

Herman, R. L., *et al.*, "Measurements of CO in the upper troposphere and lower stratosphere," *Chemosphere*, in press, 1999.

Hintsa, E. J., *et al.*, "SPADE H_2O measurements and the seasonal cycle of water vapor," *Geophys. Res. Lett.* **21**, 2559–1562, 1994.

Holton, J. R., *et al.*, "Stratosphere-troposphere exchange," *Rev. Geophys.* **33**, 405–439, 1995.

Jaeglé, L., *et al.*, "Observed OH and HO_2 in the upper troposphere suggests a major source from convective injection of peroxides," *Geophys. Res. Lett.* **24**, 3181–3184, 1997.

Kley, D., *et al.*, "*In situ* measurements of the mixing ratio of water vapor in the stratosphere," *J. Atmos. Sci.* **36**, 2513–2524, 1979.

Larabee, J. K., *Development of a Technique for In Situ Detection of Stratospheric Nitrogen Dioxide*, Ph.D. Thesis, Harvard University, October 1984.

Le Texier, H., *et al.*, "The role of molecular hydrogen and methane oxidation in the water vapor budget of the atmosphere," *Q. J. R. Meteorol. Soc.* **114**, 281–295, 1988.

Mote, P. W., *et al.*, "Seasonal variations of water vapor in the tropical lower stratosphere," *Geophys. Res. Lett.* **22**, 1093–1096, 1995

Mote, P. W., *et al.*, "An atmospheric tape recorder: The imprint of tropical tropopause temperatures on stratospheric water vapor, *J. Geophys. Res.* **101**, 2989–3006, 1996.

Newell, R. E., and S. Gould-Stewart, "A stratospheric fountain?" *J. Atmos. Sci.* **38**, 2789–2796, 1981.

Singh, H. B., *et al.*, "High concentrations and photochemical fate of oxygenated hydrocarbons in the global troposphere, *Nature* **378**, 50–54, 1995.

Singh, H. B., *et al.*, "Impact of biomass burning emissions on the composition of the South Atlantic troposphere: Reactive nitrogen and ozone," *J. Geophys. Res.* **101**, 24203–24219, 1996.

Stimpfle, R. M., *et al.*, "The response of ClO radical concentrations to variations in NO_x radical concentrations in the lower stratosphere," *Geophys. Res. Lett.* **21**, 2543–2546, 1994.

Webster, C. R., *et al.*, "Aircraft (ER-2) laser infrared absorption spectrometer (ALIAS) for *in situ* stratospheric measurements of HCl, N_2O, CH_4, NO_2, and $HONO_3$," *Applied Optics* **33**, 454–472, 1994a.

Webster, C. R., *et al.*, "Hydrochloric acid and the chlorine budget of the lower stratosphere," *Geophys. Res. Lett.* **21**, 2575–2578, 1994b.

Weinstock, E. M., *et al.*, "A new fast response photofragment fluorescence hygrometer for use on the NASA ER-2 and Perseus remotely-piloted aircraft, *Rev. Scient. Instrum.* **65**, 3544–3554, 1994.

Weinstock, E. M., E. J. Hintsa, A. E. Dessler, and J. G. Anderson, "Measurements of water vapor in the tropical lower stratosphere during the CEPEX campaign: Results and interpretation," *Geophys. Res. Lett.* **22**, 3231–3234, 1995.

Wennberg, P. O., *et al.*, "The removal of lower stratospheric ozone by free radical catalysis: *In situ* measurements of OH, HO_2, NO, NO_2, ClO, and BrO," *Science* **266**, 398–404, 1994.

OTHER PUBLICATIONS RELEVANT TO THIS RESEARCH:

1. Wennberg, P. O., T. F. Hanisco, L. Jaeglé, D. J. Jacob, E. J. Hintsa, E. J. Lanzendorf, J. G. Anderson, R. -S. Gao, E. R. Keim, S. G. Donnelly, L. Del Negro, D. W. Fahey, S. A. McKeen, R. J. Salawitch, C. R. Webster, R. D. May, R. L

Herman, M. H. Proffitt, J. J. Margitan, E. L. Atlas, C. T. McElroy, J. C. Wilson, C. A. Brock, and T. V. Bui, "Hydrogen radicals, nitrogen radicals, and the production of ozone in the middle and upper troposphere," *Science* **279**, 49–53, 1998.

2. Hintsa, E. J., P. A. Newman, H. H. Jonsson, C. R. Webster, R. D. May, R. L. Herman, L. R. Lait, M. R. Schoeberl, J. W. Elkins, P. R. Wamsley, G. S. Dutton, T. P. Bui, D. W. Kohn, and J. G. Anderson, "Dehydration and denitrification in the arctic polar vortex during the 1995–96 winter," *Geophys. Res. Lett.* **25**, 501–504 1998.
3. Hintsa, E. J., K. A. Boering, E. M. Weinstock, J. G. Anderson, B. L. Gary, L. Pfister, B. C. Daube, S. C. Wofsy, M. Loewenstein, J. R. Podolske, J. J. Margitan and T. P. Bui, "Troposphere-to-stratosphere transport in the lowermost stratosphere from measurements of H_2O, CO_2, N_2O and O_3," *Geophys. Res. Lett.* **25**, 2655–2658, 1998.
4. Hintsa, E. J., E. M. Weinstock, J. G. Anderson, R. D. May, and D. F. Hurst, "On the accuracy of in situ water vapor measurements in the troposphere and lower stratosphere with the Harvard Lyman-α hygrometer," *J. Geophys. Res.* **104**, 8183–8189, 1999.
5. Stimpfle, R. M., R. C. Cohen, G. P. Bonne, P. B. Voss, K. K. Perkins, L. C. Koch, J. G. Anderson, R. J. Salawitch, S. A. Lloyd, R. S. Gao, L. A. Del Negro, E. R. Keim, and T. P. Bui, "The coupling of $ClONO_2$, ClO and NO_2 in the lower stratosphere from *in situ* observations using the NASA ER-2 aircraft," *J. Geophys. Res.*, submitted December 1998.
6. Sen, B., G. B. Osterman, R. J. Salawitch, G. C. Toon, J. J. Margitan, J. -F. Blavier, A. Y. Chang, R. D. May, C. R. Webster, R. M. Stimpfle, G. P. Bonne, P. B. Voss, K. K. Perkins, J. G. Anderson, R. C. Cohen, J. W. Elkins, G. S. Dutton, P. A. Romashkin, D. F. Hurst, E. L. Atlas, S. M. Schauffler, and M. Loewenstein, "The budget and partitioning of stratospheric chlorine during the arctic summer, *J. Geophys. Res.*, in press, 1999.
7. Kirk-Davidoff, D., J. G. Anderson, E. J. Hintsa, and D. W. Keith, "Carbon dioxide, stratospheric water vapor and ozone depletion," *Nature*, submitted March 1999.
8. Keith, D. W., and J. G. Anderson, "Climate observation from space: The role of sensor accuracy," *J. Climate*, submitted March 1999.
9. Keith, D. W., J. A. Dykema, H. Hu, L. Lapson, and J. G. Anderson, "An airborne interferometer for atmospheric emission and solar absorption," *Applied Optics*, submitted March 1999.
10. Lazendorf, E. J., T. F. Hanisco, R. M. Stimpfle, J. G. Anderson, P. O. Wennberg, R. L. Herman, R. C. Cohen, D. W. Fahey, R. -S. Gao, C. R. Webster, R. D. May, J. J. Margitan, and T. P. Bui, "Establishing the dependence of $[HO_2]$ on temperature, halogen loading, ozone, and NO_x," *J. Geophys. Res.*, submitted 1999.
11. Perkins, K. K., T. F. Hanisco, R. C. Cohen, L. C. Koch, R. M. Stimpfle, P. B. Voss, G. P. Bonne, E. J. Lanzendorf, J. G. Anderson, P. O. Wennberg, R. -S. Gao, L. A. Del Negro, R. J. Salawitch, C. T. McElroy, E. J. Hintsa, M. Loewenstein, and T. P. Bui, "An examination of the NO_x/HNO_3 system in the lower stratosphere: Insights from *in situ* measurements during periods of continuous sunlight," *J. Geophys. Res.*, submitted 1999.
12. Hanisco, T. F., E. J. Lanzendorf, R. M. Stimpfle, G. P. Bonne, E. J. Hintsa, K. K. Perkins, R. M. Stimpfle, P. B. Voss, J. G. Anderson, P. O. Wennberg, R. Herman, R. C. Cohen, L. C. Koch, D. W. Fahey, R. -S. Gao, E. R. Keim, S. G. Donnelly, L. A. Del Negro, M. H. Proffitt, R. J. Salawitch, C. R. Webster, R. D. May, S. A. Lloyd, T. McElroy, C. Midwinter, and P. Bui, "Sources, sinks, and the distribution of OH in the lower stratosphere," *J. Geophys. Res.*, submitted 1999.
13. Bonne, G. P., R. M. Stimpfle, R. C. Cohen, P. B. Voss, K. K. Perkins, J. G. Anderson, C. R. Webster, D. C. Scott, R. D. May, R. J. Salawitch, J. W. Elkins, R. E. Dunn, G. S. Dutton, K. W. Jucks, G. C. Toon, and B. Sen, "An examination of

the inorganic chlorine budget in the lower stratosphere," *J. Geophys. Res.*, submitted 1999.

14. Bonne, G. P., R. M. Stimpfle, R. C. Cohen, P. B. Voss, K. K. Perkins, L. C. Koch, E. J. Hintsa, S. A. Lloyd, and J. G. Anderson, "*In situ* measurements of $ClONO_2$: A new thermal dissociation resonance fluorescence instrument on board the NASA ER-2 aircraft," *J. Geophys. Res.*, submitted 1999.
15. Voss, P. B., R. M. Stimpfle, T. F. Hanisco, G. P. Bonne, K. K. Perkins, E. J. Lanzendorf, J. G. Anderson, R. C. Cohen, L. C. Koch, C. R. Webster, D. C. Scott, R. D. May, R. J. Salawitch, J. J. Margitan, P. O. Wennberg, R. -S. Gao, T. P. Bui, P. A. Newman, and L. R. Lait, "Chlorine partitioning in the summer lower stratosphere: A comparison of modeled and measured chlorine partitioning during POLARIS," *J. Geophys. Res.*, submitted 1999.
16. Smith, J. B., E. J. Hintsa, and J. G. Anderson, "Mechanisms for midlatitude ozone loss: Cirrus clouds in the stratosphere?" *J. Geophys. Res.*, submitted 1999.